

The Power Spectrum, Bias Evolution, and the Spatial Three-Point Correlation Function

Ari Buchalter^{*1} and Marc Kamionkowski^{†2}

^{*}Department of Astronomy and Columbia Astrophysics Laboratory, Columbia University,
538 West 120th Street, New York, NY 10027

[†]Department of Physics and Columbia Astrophysics Laboratory, Columbia University, 538
West 120th Street, New York, NY 10027

ABSTRACT

We calculate perturbatively the normalized spatial skewness, S_3 , and full three-point correlation function (3PCF), ζ , induced by gravitational instability of Gaussian primordial fluctuations for a biased tracer-mass distribution in flat and open cold-dark-matter (CDM) models. We take into account the explicit dependence on cosmological parameters, the shape and evolution of the CDM power spectrum, and allow the bias to be nonlinear and/or evolving in time, using an extension of Fry's (1996) bias-evolution model. We derive a scale-dependent, leading-order correction to the standard perturbative expression for S_3 (Fry & Gaztañaga 1993) in the case of nonlinear biasing, as defined for the unsmoothed galaxy and dark-matter fields, and find that this correction becomes large when probing positive effective power-spectrum indices, i.e., scales above $100 h^{-1}$ Mpc for reasonable CDM models. This term implies that the inferred nonlinear-bias parameter, as usually defined in terms of the smoothed density fields, might in general depend on the chosen smoothing scale, and could allow better constraints on both the linear- and nonlinear-bias parameters on the basis of skewness measurements alone (or at least distinguish between the smoothed and unsmoothed bias pictures), if S_3 could be measured over very large scales. In general, we find that the dependence of S_3 on the biasing scheme can substantially outweigh that on the adopted cosmology, with linear and nonlinear bias separately giving rise to distinct signatures in

¹ari@astro.columbia.edu

²kamion@phys.columbia.edu

the skewness, but degenerate ones in combination. We demonstrate that the normalized 3PCF, Q , is an ill-behaved quantity, and speculate that reported discrepancies between perturbative and N -body predictions for Q may arise in part from systematic errors associated with the poor choice of normalization. To avoid this problem we investigate Q_V , the variance-normalized 3PCF. The configuration dependence of Q_V shows similarly strong sensitivities to the bias scheme as S_3 , but also exhibits significant dependence on the form of the CDM power spectrum. Though the degeneracy of S_3 with respect to the cosmological parameters and constant linear- and nonlinear-bias parameters can be broken by the full configuration dependence of Q_V , neither statistic can distinguish well between evolving and non-evolving bias scenarios, since an evolving bias is found to effectively mimic a smaller but constant bias. We show that this can be resolved, in principle, by considering the redshift dependence of ζ which can also yield direct constraints on Ω_0 and the epoch of galaxy formation.

Subject headings: large scale structure of the universe — cosmology: theory — galaxies: clustering — galaxies: statistics

1. INTRODUCTION

Recovery of the primordial distribution of density perturbations is crucial to understanding the origin of large-scale structure. Inflation, possibly the most promising paradigm for the origin of structure, predicts Gaussian initial conditions (ICs), while most alternative models generally predict some deviation from Gaussianity. It is well known that gravitational instability will induce non-Gaussianity in an initially Gaussian distribution of cosmological perturbations, as the nonlinear collapse process gives rise to interactions between initially uncoupled modes and thus to non-zero higher-order moments. As fluctuations become nonlinear on progressively larger scales, larger objects become virialized, producing a hierarchy of structure. In the quasi-linear (QL) regime, where the rms fluctuations are small compared to unity, perturbative solutions to the fluid equations for a self-gravitating pressureless fluid in an expanding universe can be used to derive the resulting n -point correlation functions³ (CFs) and their Fourier-space counterparts, the polyspectra, induced by gravitational instability (Peebles 1980; Fry 1984; Goroff et al. 1986). In particular, the three-point correlation function (3PCF), or equivalently, its

³“Correlation function” refers throughout to the connected, or reduced, correlation function.

Fourier transform (FT), the bispectrum, is the lowest-order intrinsically nonlinear statistic and can therefore place strong constraints on models of structure formation⁴.

The perturbation-theory (PT) calculation predicts so-called hierarchical behavior of the polyspectra, whereby those of higher order can be simply related to the power spectrum, since the physics on QL scales is still determined entirely by the ICs. In the case of the bispectrum,

$$B(k_1, k_2, k_3) = \mathcal{Q}(k_1, k_2, k_3) [P(k_1)P(k_2) + P(k_2)P(k_3) + P(k_3)P(k_1)], \quad (1)$$

where $P(k)$ is the power spectrum and \mathcal{Q} is of order unity and depends only on the magnitudes, $k_i = |\mathbf{k}_i|$, of the three wave vectors forming a triangle in k -space. (Fry 1984; Goroff et al. 1986). A similar form was proposed, on purely empirical grounds, by Peebles (1974, 1975, 1980) for the spatial 3PCF,

$$\zeta(r_{12}, r_{23}, r_{31}) = Q(r_{12}, r_{23}, r_{31}) [\xi(r_{12})\xi(r_{23}) + \xi(r_{12})\xi(r_{31}) + \xi(r_{23})\xi(r_{31})], \quad (2)$$

where $\xi(r)$ is the two-point correlation function (2PCF) and the normalized amplitude, Q , depends only on the physical separations, $r_{ij} = |\mathbf{r}_i - \mathbf{r}_j|$, of the three points in real space given by coordinates \mathbf{r}_i , and is assumed to be of order unity. It should be noted that though many authors assume Q to be a constant, this is strictly untrue, nor is Q given by the k -space \mathcal{Q} ; rather it is a function defined by equation (2), independent of the validity of the hierarchical model. A related, more tractable statistic which is commonly used is the normalized spatial skewness, $S_3(R)$, related to Q evaluated at zero lag for a distribution smoothed over an effective scale half-width R .

Studies of the spatial 3PCFs of different tracer populations on small scales (i.e., below $10 h^{-1}$ Mpc) have generally yielded results consistent with the assumed hierarchical form above, i.e., values of $Q \approx 1 \pm 0.5$ (Groth & Peebles 1977; Jing & Zhang 1989; Tóth, Hollósi, & Szalay 1989; Gott, Gao, & Park 1991; Jing, Mo, & Börner 1991; Baumgart & Fry 1991; Bouchet et al. 1993; Jing & Börner 1998) and values of S_3 of order a few (Gaztañaga 1992; Bouchet et al. 1993; Cappi & Maurogordato 1995; Gaztañaga, Croft, & Dalton 1995), and numerical simulations have also lent support to the hierarchical model (Bouchet, Schaeffer, & Davis 1991; Fry, Melott, & Shandarin 1993, 1995; Bernardeau 1994a; Baugh, Gaztañaga, & Efstathiou 1995; Colombi, Bouchet, & Hernquist 1996). At larger scales, however, the detailed behavior of these higher-order statistics, such as the configuration-dependence of

⁴ Note that the n -point CFs are valid statistics only if the universe is homogeneous on large scales (as opposed to exhibiting, say, multi-fractal structure). We invoke the assumptions of large-scale homogeneity and isotropy, so that the CFs depend only relative distances and are independent of orientation.

Q , is not well constrained. Often, results for Q are quoted as constant simply because they reflect averages over all geometries, thus wiping out valuable information. Jing & Börner (1997, hereafter JB97) and Matsubara & Suto (1994) do investigate the shape dependence of Q , but find substantial disagreement between the predictions of QL PT and those of N -body simulations. Jing & Börner (1998) further find significant deviations between the observed configuration dependence of Q_{proj} , the projected Q perpendicular to the line of sight, and the standard hierarchical result. These differences may be attributable to various mechanisms, such as nonlinear effects, finite volume effects, and projection effects, which can reduce the configuration dependence of both observed and N -body results for Q , as compared with QL PT predictions. The observed discrepancies, however, might also suggest that problems exist in the definition of Q .

That the normalized amplitudes Q and S_3 have been observed to exhibit roughly stable values near unity, as predicted, over scales on which ζ and ξ individually vary by many orders of magnitude, has been interpreted as loose support for the scenario of gravitational evolution of Gaussian ICs. It is clear, however, that the uncertainties in theoretical models, as well as in the data, are still appreciable. Much of this uncertainty is due to the fact that existing redshift surveys have not been both large and deep enough to yield strong constraints, particularly on QL scales. However, with the advent of new, deep surveys at various wavelengths (radio, optical, infra-red, x-ray), probing many different populations (galaxies, quasars, clusters, etc.), a rapidly growing database of spectroscopic and photometric redshifts, and powerful new computing resources, it will soon be possible to achieve precise measurements of higher-order spatial CFs. Interpreting the data from these upcoming surveys will require more realistic modeling of a variety of effects which may enter into the theoretical calculations. For example, the 3PCF can depend on the detailed form of the power spectrum (Frieman & Gaztañaga 1994; JB97) and, particularly for the case of angular CFs (see Buchalter, Kamionkowski, & Jaffe 1999, hereafter BKJ), on the density of nonrelativistic matter, the cosmological constant, Λ , or the density of some other form of matter (Bouchet et al. 1992; Bernardeau 1994a; Bouchet et al. 1995; Catelan et al. 1995; Martel 1995; Scoccimarro et al. 1998; Kamionkowski & Buchalter 1998). Furthermore, smoothing of the density field, as occurs when determining S_3 from the moments of counts-in-cells, must be taken into account (Bernardeau 1994a,b). Perhaps most importantly, however, biasing of the tracer population will have a significant effect on the observed 3PCF (Fry 1984; Fry & Gaztañaga 1993, hereafter FG93).

Bias—the notion that observed structures do not exactly trace the underlying density field—is advocated by both theory and observations, and may in general be scale and/or time dependent. In deterministic models, the fractional density perturbation $\delta(\mathbf{r})$ of the unsmoothed tracer-mass distribution may be expanded in terms of the perturbation $\delta_m(\mathbf{r})$

to the total mass distribution,

$$\delta(\mathbf{r}) = b_1 \delta_m(\mathbf{r}) + \frac{b_2}{2} [\delta_m(\mathbf{r})]^2 + \cdots, \quad (3)$$

where b_1 is the linear bias term, b_2 the first nonlinear term, etc., and δ_m is itself written as $\delta_m = \delta_m^{(1)} + \delta_m^{(2)} + \cdots$, where $\delta_m^{(n)} \ll \delta_m^{(n-1)}$, $\delta_m^{(1)}$ is the linear solution, and $\delta_m^{(2)}$ is the leading-order departure from the Gaussian ICs. Note that the bias terms defined above are scale-independent, since equation (3) is a local relation between the unsmoothed density fields at every point (we comment further on this assumption below). Like gravitational evolution or primordial skewness, the existence of nonlinear bias will also give rise to a non-zero third moment in the present-day density distribution of the tracer mass (since the 3PCF is intrinsically second order, and thus requires the b_2 term in the PT calculation). These effects cannot be reliably distinguished by present data. Furthermore, though Gaussian ICs are sufficient to produce hierarchical behavior, they are not necessary; even if the data are shown to follow the predicted hierarchy to high accuracy, it is possible that this result is merely a coincidence of the bias. The impact of bias and its variation (thought to be primarily with redshift) on the 3PCF must therefore be taken into account if the predictions of Gaussian ICs are to be tested unambiguously. It has been shown that the detailed behavior of the 3PCF can constrain the initial density profile (Fry & Scherrer 1994; Heavens 1998), distinguish between contributions to clustering from gravitational collapse vs. bias (Szalay 1988; FG93; Fry 1994; Frieman & Gaztañaga 1994) and, for a given tracer population, yield determinations of the linear and nonlinear bias parameters (Frieman & Gaztañaga 1994; Gaztañaga & Frieman 1994; Jing 1997; Matarrese, Verde, & Heavens 1997). Moreover, if different populations, such as clusters and galaxies, are differently biased relative to the underlying mass distribution, then measuring the 3PCFs of these populations can provide multiple, independent constraints. Several authors have recently argued that bias, and its evolution, is the dominant consideration in evaluating structure-formation models against clustering data, and have pointed to the need for employing more sophisticated bias models than the simplest ones often used (i.e., local, linear, and non-evolving) (JB97, Jing & Börner 1998; Bernardeau 1995; Matarrese et al. 1997).

In this paper, we calculate the normalized spatial skewness, $S_3(R)$, and normalized 3PCF, $Q(\mathbf{r}_1, \mathbf{r}_2, \mathbf{r}_3)$, in the QL regime assuming Gaussian ICs. We consider open and flat cosmological models with arbitrary allowed values of Ω_0 and Ω_Λ , and take into account the dependence on the detailed form and evolution of the CDM power spectrum. We further include the effect of linear and nonlinear bias, and in particular, their time evolution, via an extension of the Fry (1996) bias-evolution model to the case of an arbitrary expansion history (BKJ perform similar calculations to obtain corresponding results for the angular

skewness and 3PCF). For comparison, we derive the results for S_3 with a power-law spectrum, including a scale-dependent, leading-order correction to the standard expression for S_3 (FG93) in the case of a nonlinear bias as defined in equation (3). This correction term becomes appreciable for positive effective spectral indices, corresponding to scales $R \gtrsim 100 h^{-1}$ Mpc for CDM models. The existence of this term implies that the value of the nonlinear-bias parameter, as defined for *smoothed* density fields, could in general depend on the adopted smoothing scale. For a given CDM model, this dependence, in principle, would allow a more accurate determination of the linear- and nonlinear-bias parameters on the basis of skewness measurements alone, provided however, that S_3 could be measured over sufficiently large scales. We show that Q is a poorly-defined statistic, exhibiting rapid variation and divergences which do not arise from the behavior of the 3PCF itself, but are rather due to the quantity $[\xi(r_{12})\xi(r_{23}) + \xi(r_{12})\xi(r_{31}) + \xi(r_{23})\xi(r_{31})]$ in equation (2) acquiring values of or near zero in various cases [the k -space Q defined in equation (1) is not subject to this normalization problem]. This dramatic behavior of Q is in marked contrast to that predicted by some N -body simulations (JB97; Matsubara & Suto 1994) and we propose that this discrepancy is due at least in part to the practical inability to measure CFs to high precision near zero. We suggest that this may be addressed by considering N -body results for Q at earlier epochs, where nonlinear effects can be safely ignored; to avoid this problem altogether, we define the variance-normalized 3PCF, Q_V , given by ζ divided by the square of the variance at a given scale. We find that S_3 and Q_V do indeed depend strongly on the bias scheme, as has been suggested. In particular, a significant linear (nonlinear) bias term produces a relative decrease (increase) in both normalized amplitudes, and a significant linear term is found to reduce the variation of S_3 with smoothing scale and of Q_V with triangle geometry, as compared with the unbiased predictions. While S_3 is found to be only mildly sensitive to the cosmological parameters, Q_V can vary appreciably with the value of the parameter $\Gamma \simeq \Omega_0 h$, determined by the epoch of matter-radiation equality, that locates the peak in the power spectrum. In general, Q_V is found to depend strongly on the triangle geometry, with smaller, elongated structures, corresponding to filaments or sheets, being more strongly clustered. The rich configuration dependence of the 3PCF is shown to break the degeneracy present in S_3 on scales $R < 100 h^{-1}$ Mpc, between the cosmological parameters and in particular the constant linear- and nonlinear-bias parameters. Both statistics, however, are unable to distinguish well between models of evolving and non-evolving bias, since an evolving bias effectively acts as a smaller, constant bias. We show that measurements of bias evolution, as well as of Ω_0 and the epoch of galaxy formation, could potentially be isolated by considering ζ as a function of redshift in a very deep ($\bar{z} > 1$) survey. Alternatively, BKJ show that similar results can be obtained more feasibly from measurements of the angular 3PCF.

2. SPATIAL SKEWNESS

The results below are based on leading-order PT and are thus restricted to the QL regime, where $\xi \lesssim 1$. Though the leading-order contributions to higher moments of the density distribution are appreciable at these scales, higher-order nonlinear contributions are not expected to be significant, and various authors have shown that observations and simulations in this regime are well-matched by leading-order results alone (Szalay 1988; Tóth, Hollósi, & Szalay 1989; Gott, Gao, & Park 1991; Bouchet, Schaeffer, & Davis 1991; Fry, Melott, & Shandarin 1993, 1995; Colombi, Bouchet, & Hernquist 1996; Scoccimarro et al. 1998). In addition, numerical simulations suggest that large scales still obey leading-order PT even when small scales have become fully nonlinear (Bouchet & Hernquist 1992; Fry, Melott, & Shandarin 1995), and further that the results of QL PT hold even on scales where the rms fluctuation is $\gtrsim 1$ (Bernardeau 1994a; Baugh, Gaztañaga, & Efstathiou 1995; Fry, Melott, & Shandarin 1995).

We wish to derive an expression for the normalized 3PCF, Q , defined in equation (2), for a distribution of tracer masses, such as galaxies, clusters, or radio sources. This quantity has the advantage that it is independent of the overall normalization of the power spectrum. The full spatial 3PCF is given by $\zeta(\mathbf{r}_1, \mathbf{r}_2, \mathbf{r}_3) \equiv \langle \delta(\mathbf{r}_1) \delta(\mathbf{r}_2) \delta(\mathbf{r}_3) \rangle$, where \mathbf{r} is the comoving position and $\delta(\mathbf{r}) = [\rho(\mathbf{r}, t_0) - \bar{\rho}(t_0)]/\bar{\rho}(t_0)$ is the present fractional perturbation to the unsmoothed tracer-mass density. Although the spatial 3PCF is nominally the function of nine quantities, statistical homogeneity and isotropy guarantee that the 3PCF depends only on three parameters which may be taken to be, e.g., the three distances between the three points. Still, evaluating Q over all allowed configurations may be fairly complicated, so it has become increasingly popular to focus instead on the normalized skewness $S_3 \equiv \langle \delta^3(r) \rangle \langle \delta^2(r) \rangle^{-2}$. This statistic is likewise independent of the power-spectrum normalization and is far easier to calculate than its full n -point counterpart, while still preserving much of the information contained therein.

In practice, $\delta(\mathbf{r})$ cannot be evaluated continuously, since the observed tracer-mass distribution is discrete, so we define $\delta_R(\mathbf{r})$ to be the density contrast smoothed over a cell with an effective comoving scale half-width R .⁵ In particular, we shall choose a spherical top-hat window function; in terms of the Fourier components, $\tilde{\delta}(\mathbf{k})$, of the unsmoothed density field,

$$\delta_R(\mathbf{r}) = \int \frac{d^3\mathbf{k}}{(2\pi)^3} \tilde{\delta}(\mathbf{k}) e^{i\mathbf{k}\cdot\mathbf{r}} W(kR), \quad (4)$$

⁵ We implicitly assume $\delta = \frac{\rho}{\bar{\rho}} - 1 \propto \frac{n}{n} - 1$, where n is the number of discrete counts.

where $W(x) = 3\sqrt{\pi/2} x^{-3/2} J_{3/2}(x)$ is the FT of the three-dimensional spherical top-hat window function and $J_n(x)$ is a Bessel function of order n . Since we are working in the regime where $\langle \delta^2 \rangle \ll 1$, fluctuations at or below the smoothing scale will not significantly affect our results (Bernardeau 1994a,b; see §3).

The counts-in-cells spatial 2PCF is then given by

$$\xi_R(r_{12}) = \langle \delta_R(\mathbf{r}_1) \delta_R(\mathbf{r}_2) \rangle = \int \int \frac{d^3 \mathbf{k}_1}{(2\pi)^3} \frac{d^3 \mathbf{k}_2}{(2\pi)^3} e^{i(\mathbf{k}_1 \cdot \mathbf{r}_1 + \mathbf{k}_2 \cdot \mathbf{r}_2)} W(k_1 R) W(k_2 R) \langle \tilde{\delta}(\mathbf{k}_1) \tilde{\delta}(\mathbf{k}_2) \rangle. \quad (5)$$

The power spectrum of the tracer mass, $P(k, t)$, is defined via

$$\langle \tilde{\delta}(\mathbf{k}_1) \tilde{\delta}(\mathbf{k}_2) \rangle \equiv (2\pi)^3 \delta_D(\mathbf{k}_1 + \mathbf{k}_2) P(k, t), \quad (6)$$

where δ_D is the Dirac delta function and $k = |\mathbf{k}_1|$. Putting this into equation (5), we have

$$\langle \delta_R(\mathbf{r}_1) \delta_R(\mathbf{r}_2) \rangle = \int \frac{d^3 \mathbf{k}}{(2\pi)^3} e^{i(\mathbf{k} \cdot \mathbf{r}_{12})} P(k, t) W^2(kR), \quad (7)$$

where one integral vanishes under the requirement $\mathbf{k}_1 = -\mathbf{k}_2$, $\mathbf{r}_{12} = \mathbf{r}_1 - \mathbf{r}_2$, and we have made use of the even symmetry of the window function. Taking $\mathbf{r}_1 = \mathbf{r}_2 \equiv \mathbf{r}$, we obtain an expression for the variance,

$$\xi_R(0) = \langle \delta_R^2(\mathbf{r}) \rangle = \int \frac{d^3 \mathbf{k}}{(2\pi)^3} P(k, t) W^2(kR). \quad (8)$$

The linear solution to the equations of motion for the underlying density contrast has the separable form,

$$\delta_m^{(1)}(\mathbf{r}, t) = D(t) \delta_m^{(1)}(\mathbf{r}, 0), \quad (9)$$

where $D(t)$ is the linear-theory growth factor, given (as a function of redshift) by

$$D(z) = \frac{5\Omega_0 E(z)}{2} \int_z^\infty dz' \frac{1+z'}{[E(z')]^3}, \quad E(z) = \sqrt{\sum_i \Omega_i (1+z)^{3(1+w_i)}}, \quad (10)$$

where $\sum_i \Omega_i = 1$ and Ω_i represents the contribution to the overall energy density from species i having equation of state $p = w_i \rho$,⁶ for an Einstein de-Sitter universe, $D(t)$ is simply the scale factor, $a(t)$. One can then see from equation (6) that the spatial and time

⁶In this formulation, the curvature of the universe contributes an amount Ω_K to the total energy density, and yields the term $\Omega_K(1+z)^2$ in the sum in equation (10); Thus, in a universe with, for example, a ratio of nonrelativistic-matter density to closure density of Ω_0 and a cosmological-constant contribution to the total density of Ω_Λ , $E(z) = \sqrt{\Omega_0(1+z)^3 + \Omega_\Lambda + (1 - \Omega_0 - \Omega_\Lambda)(1+z)^2}$.

dependence of the power spectrum can likewise be separated. Assuming the unsmoothed tracer-mass density contrast to be related to the total-mass distribution via equation (3), we write the leading-order result for the power spectrum of the unsmoothed tracer-mass fluctuations as

$$P(k, t) = Ab_1^2 D^2(t) k^n T^2(k), \quad (11)$$

where A is the overall amplitude and $T(k)$ is a model-dependent transfer function. Substituting equation (11) into (8), setting $x = kR$, and performing the angular integrations, we have

$$\xi_R(0) = \langle \delta_R^2(\mathbf{r}) \rangle = \frac{2Ab_1^2 D^2(t)}{(2\pi)^2 R^{n+3}} \int_0^\infty dx x^{n+2} T^2(x/R) W^2(x). \quad (12)$$

We now follow a similar procedure for the counts-in-cells 3PCF,

$$\begin{aligned} \zeta_R(r_{12}, r_{23}, r_{31}) &= \langle \delta_R(\mathbf{r}_1) \delta_R(\mathbf{r}_2) \delta_R(\mathbf{r}_3) \rangle = \int \int \int \frac{d^3 \mathbf{k}_1}{(2\pi)^3} \frac{d^3 \mathbf{k}_2}{(2\pi)^3} \frac{d^3 \mathbf{k}_3}{(2\pi)^3} e^{i(\mathbf{k}_1 \cdot \mathbf{r}_1 + \mathbf{k}_2 \cdot \mathbf{r}_2 + \mathbf{k}_3 \cdot \mathbf{r}_3)} \\ &\times \langle \tilde{\delta}(\mathbf{k}_1) \tilde{\delta}(\mathbf{k}_2) \tilde{\delta}(\mathbf{k}_3) \rangle W(k_1 R) W(k_2 R) W(k_3 R). \end{aligned} \quad (13)$$

The bispectrum, B , of the unsmoothed tracer-mass distribution is defined via

$$\langle \tilde{\delta}(\mathbf{k}_1) \tilde{\delta}(\mathbf{k}_2) \tilde{\delta}(\mathbf{k}_3) \rangle \equiv (2\pi)^3 \delta_D(\mathbf{k}_1 + \mathbf{k}_2 + \mathbf{k}_3) B(k_1, k_2, k_3, t), \quad (14)$$

and is given, to leading order in PT, by (Fry 1984; Goroff et al. 1986; Matarrese, Verde, & Heavens 1997)

$$\begin{aligned} B(k_1, k_2, k_3, t) &= P(k_1, t) P(k_2, t) \left\{ \frac{1}{b_1} \left[1 + \mu + \cos \theta \left(\frac{k_1}{k_2} + \frac{k_2}{k_1} \right) + (1 - \mu) \cos^2 \theta \right] \right. \\ &\quad \left. + \frac{b_2}{b_1^2} \right\} + (\text{cyc.}), \end{aligned} \quad (15)$$

where θ is the angle between \mathbf{k}_1 and \mathbf{k}_2 , and μ is a function of the expansion history (Bouchet et al. 1992; Bernardeau 1994a; Bouchet et al. 1995; Catelan et al. 1995; Martel 1995; Scoccimarro et al. 1998; Kamionkowski & Buchalter 1998). For an Einstein-de Sitter universe, $\mu = 3/7$ (Peebles 1980). Bouchet et al. (1992) derive the approximation $\mu \simeq (3/7) \Omega_0^{-2/63}$ for an open universe. Kamionkowski & Buchalter (1998) find $\mu \simeq (3/7) \Omega_0^{-1/140}$ for a flat universe with a cosmological constant [see also Bouchet et al. (1995)]. Bernardeau (1994a), Catelan et al. (1995), and Scoccimarro et al. (1998) give analytical arguments that further show that μ will depend only very weakly on the expansion history, and Kamionkowski & Buchalter (1998) verify this numerically for a variety of models. For plausible models with $\Omega_0 \geq 0.1$, the corrections to μ are below 2%

but we include them here for completeness. Note that the expression for B includes the dependence on the nonlinear bias term b_2 , since the first non-trivial terms in the connected n -point CFs require PT to order $n - 1$ [cf. equation (3)]. Setting $\mathbf{r}_1 = \mathbf{r}_2 = \mathbf{r}_3 \equiv \mathbf{r}$, $x_i = k_i R$, taking \mathbf{k}_1 to lie in the $\theta = 0$ direction, and inserting equations (14) and (15) into (13), we obtain the skewness,

$$\begin{aligned} \langle \delta_R^3(\mathbf{r}) \rangle &= \frac{6A^2 b_1^4 D^4(t)}{(2\pi)^4 R^{2n+6}} \int_0^\infty dx_1 x_1^{n+2} T^2(x_1/R) W(x_1) \int_0^\infty dx_2 x_2^{n+2} T^2(x_2/R) W(x_2) \\ &\times \int_0^\pi d\theta \sin \theta \left\{ \frac{1}{b_1} \left[(1 + \mu) + \cos \theta \left(\frac{x_1}{x_2} + \frac{x_2}{x_1} \right) + (1 - \mu) \cos^2 \theta \right] + \frac{b_2}{b_1^2} \right\} W(x_3), \end{aligned} \quad (16)$$

where a factor of 3 arises from symmetry considerations applied to the 2 permutations in equation (15). Noting that $x_3 = \sqrt{x_1^2 + x_2^2 + 2x_1 x_2 \cos \theta}$, we can evaluate the θ integral by using summation theorems for Bessel functions (Gradshteyn & Ryzhik 1980; Bernardeau 1994a) which lead to the following relations:

$$\int_0^\pi d\theta \sin^3 \theta W(x_3) = \frac{4}{3} W(x_1) W(x_2), \quad (17)$$

$$\int_0^\pi d\theta \sin \theta \left(1 + \frac{x_2}{x_1} \cos \theta \right) W(x_3) = \frac{2}{3} X(x_2) W(x_1), \quad (18)$$

$$\int_0^\pi d\theta \sin \theta W(x_3) = \frac{4}{3} \sum_{j=0}^\infty (2j + 3/2) W_{2j+3/2}(x_1) W_{2j+3/2}(x_2), \quad (19)$$

where $X(x) = 3 \sin x/x$ and $W_n(x) \equiv 3\sqrt{\pi/2} x^{-3/2} J_n(x)$, so that $W(x) = W_{3/2}(x)$. Thus, we have

$$\begin{aligned} \langle \delta_R^3(\mathbf{r}) \rangle &= \frac{12A^2 b_1^2 D^4(t)}{(2\pi)^4 R^{2n+6}} \int_0^\infty dx_1 x_1^{n+2} T^2(x_1/R) W(x_1) \int_0^\infty dx_2 x_2^{n+2} T^2(x_2/R) W(x_2) \\ &\times \left(\frac{1}{b_1} \left[\frac{1}{3} X(x_1) W(x_2) + \frac{1}{3} X(x_2) W(x_1) \right] - \frac{2}{3} \frac{(1 - \mu)}{b_1} W(x_1) W(x_2) \right. \\ &\left. + \frac{2}{3} \frac{b_2}{b_1^2} \sum_{j=0}^\infty (2j + 3/2) W_{2j+3/2}(x_1) W_{2j+3/2}(x_2) \right). \end{aligned} \quad (20)$$

For a given choice of b_1 and b_2 , the skewness obtained from equations (12) and (20) effectively depends only on the smoothing radius, R and the form of the power spectrum; the explicit dependence on Ω_0 and Ω_Λ (through the dependence of μ) is very weak.

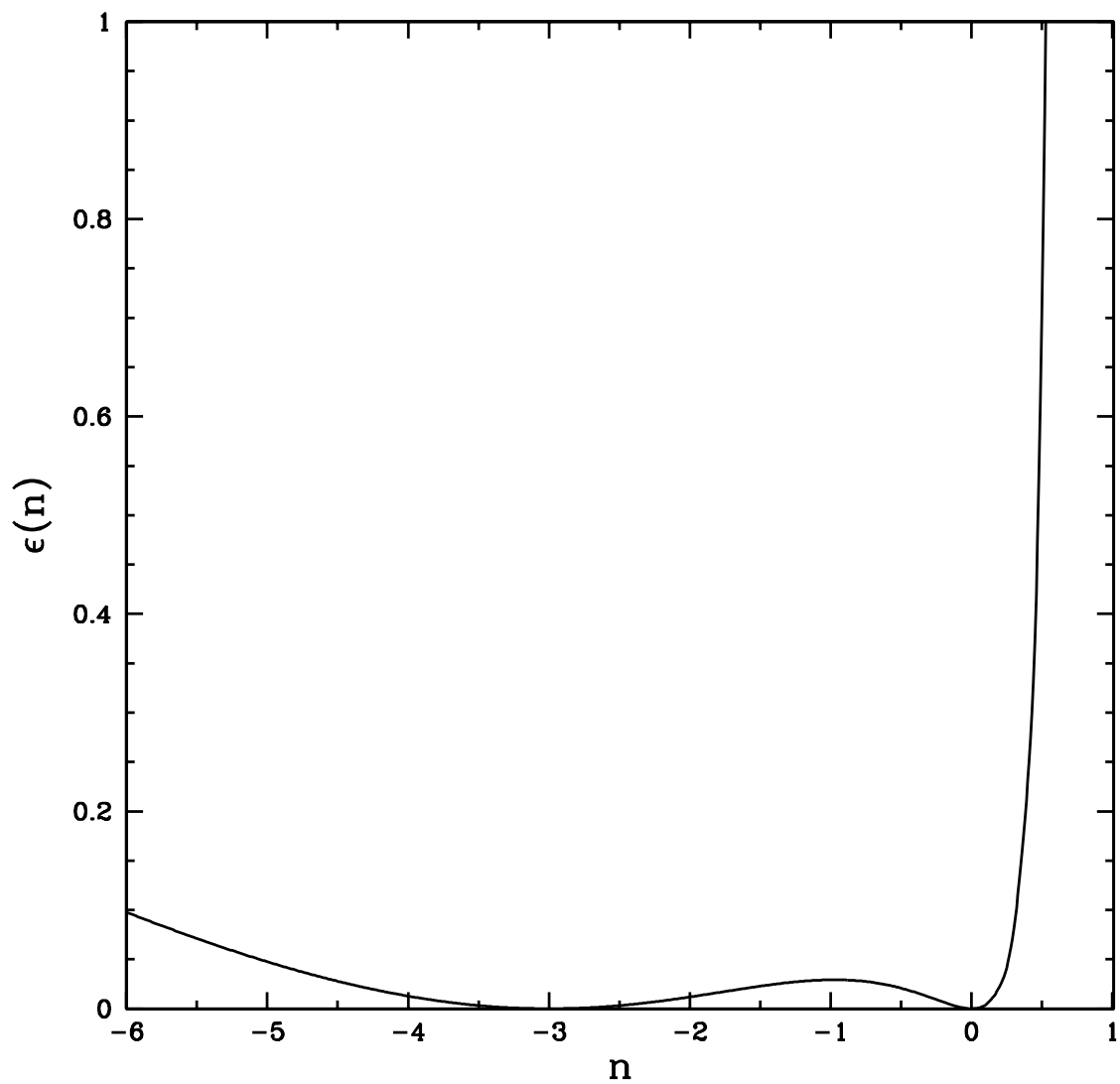


Fig. 1.— The function $\epsilon(n)$ from equation (23). For $-3 < n < 0$ the contribution of this term to S_3 in equation (22) is negligible, but increases rapidly for $n > 0$, due to the increased weighting of small-scale fluctuations by the unbounded power-law spectrum.

2.1. Effects of The Power Spectrum

In general, we will consider a CDM transfer function given by (Bardeen et al. 1986)

$$T(q) = \frac{\ln(1 + 2.34q)/(2.34q)}{[1 + 3.89q + (16.1q)^2 + (5.46q)^3 + (6.71q)^4]^{1/4}}, \quad (21)$$

where $q = k_p/\Gamma$, $\Gamma \simeq \Omega_0 h$, and k_p is the physical wavenumber in units of $h \text{ Mpc}^{-1}$. The result for S_3 is then obtained by using equation (21) together with (20) and (12). It is instructive to compare the CDM results with those obtained assuming a power-law power spectrum, $P(k) \propto k^n$. In this case, the x -integrals associated with the first two terms in parentheses in equation (20) can be evaluated analytically, and we obtain:

$$S_3 = \frac{\langle \delta_R^3(\mathbf{r}) \rangle}{\langle \delta_R^2(\mathbf{r}) \rangle^2} = \frac{1}{b_1} \left[\frac{34}{7} + \frac{6}{7} \left(\frac{7}{3}\mu - 1 \right) - (3 + n) \right] + 3 \frac{b_2}{b_1^2} [1 + \varepsilon(n)], \quad (22)$$

where

$$\varepsilon(n) = \frac{2}{3} \sum_{j=1}^{\infty} (2j + 3/2) \frac{\left[\int_0^{\infty} dx x^{n-1} J_{3/2}(x) J_{2j+3/2}(x) \right]^2}{\left[\int_0^{\infty} dx x^{n-1} J_{3/2}(x) J_{3/2}(x) \right]^2}. \quad (23)$$

Equations (22) and (23) are valid for n in the range $-3 < n < 1$. The individual terms in the sum in equation (23) can be evaluated explicitly (Watson 1966), and we find that $\varepsilon(n) \ll 1$ for $-3 < n < 0$, but diverges for $n > 0$, as demonstrated in Figure 1. Like the $(3 + n)$ term, the $\varepsilon(n)$ term [which arises from the term proportional to b_2 in equation (20)] reflects the effect of the smoothing filter on the biased, contiguous field, $\delta(\mathbf{r})$, defined in equation (3). The filter is designed to separate smooth, large-scale fluctuations from the nonlinear, small-scale field. However, a nonlinear distribution having a scale-free power spectrum with $n > 0$ contains so much small-scale power that the deviations induced by smoothing over these small-scale fluctuations become comparable to, or greater than, the perturbations above the smoothing scale, thus leading to the divergence in $\varepsilon(n)$.

The form of equation (22) agrees with the previously known scale-free result for S_3 for a constant, nonlinear bias (Bouchet et al. 1992; Juszkiewicz, Bouchet, & Colombi 1993; FG93; Bernardeau 1994a; Fry 1994), with the exception of the $\varepsilon(n)$ term. This difference arises from the fact that other authors calculating higher-order moments of the smoothed tracer-mass field (e.g., FG93) typically define the bias parameters using the form of equation (3) to relate the *smoothed* tracer-mass and total-mass fields, i.e.,

$$\delta_R = b_1^{(s)} \delta_{m_R} + \frac{b_2^{(s)}}{2} (\delta_{m_R})^2 + \dots, \quad (24)$$

where the $b_i^{(s)}$ are the “smoothed bias” terms and a subscripted R again denotes a smoothed field. Biasing and smoothing do not commute; whereas the unsmoothed bias parameters

we define in equation (3) are truly local and scale-independent, the definition of bias in equation (24) is inherently non-local, only fixing the smoothed bias parameters at the chosen smoothing scale. While it can be shown, using perturbation theory, that $b_1^{(s)} = b_1$, the higher-order smoothed bias terms will in general be different from their constant-valued counterparts in equation (3), and the magnitude of the difference will depend on the scale on which the $b_i^{(s)}$ are defined. Had we used the smoothed bias parameters as defined in equation (24), we would recover the result of FG93, i.e., equation (22) with $b_1 \rightarrow b_1^{(s)}$, $b_2 \rightarrow b_2^{(s)}$, and $\varepsilon(n) = 0$. Comparing our result for S_3 with that of FG93, we can infer that $b_2^{(s)} = b_2[1 + \varepsilon(n)]$. In the no-smoothing limit, corresponding to $n \rightarrow -3$, we recover $b_2^{(s)} = b_2$, as expected.

Of course, the unsmoothed bias parameters are defined only in the fictitious limit of continuous density fields. In practice, one might expect the efficiency of galaxy formation to depend on the matter density not only at the point of interest, but in the neighboring vicinity as well. Models such as peak biasing and halo biasing (Mo & White 1996) in fact imply a biasing relation such as equation (24), where the smoothed bias parameters do in fact tend towards constant values in the large-scale limit. Such a scenario would thus be inconsistent with the definition of the unsmoothed bias parameters in equation (3), and would yield precisely the FG93 result for S_3 , rather than equation (22). Fortunately, these two situations can be distinguished on the basis of the large-scale behavior of S_3 , as we will illustrate. Unless otherwise stated, it is hereafter understood that bias shall refer to the relationship between the unsmoothed tracer-mass and dark-matter fields, as given by equation (3).

Naturally, equation (22) is R -independent, as expected for a scale-free power spectrum. While the actual power spectrum for any tracer-mass distribution will not be simply a scale-free power law with $n > 0$, it may be wondered whether, in the unsmoothed biasing picture, the divergence seen in Figure 1 will affect the results for S_3 on scales where the slope of the true (CDM) power spectrum is positive. Bernardeau (1994a) shows that the scale-dependent CDM result, without bias, can be recovered by using an effective index,

$$n_R \equiv -\frac{d \log \xi_R(0)}{d \log R} - 3, \quad (25)$$

in place of n in the scale-free result for S_3 .⁷ If we assume, for the sake of argument, that this holds true when calculating S_3 assuming our nonlinear biasing model, we can illustrate

⁷By contrast, using an effective index defined by $n_k \equiv [d \log P(k)]/d \log k$, evaluated at wavenumber $k = c/R$ (where c is constant of proportionality chosen as to yield the best-fitting results), yields fractional errors in S_3 of at least 5% (20%) for the smallest (largest) scales shown in Figure 2.

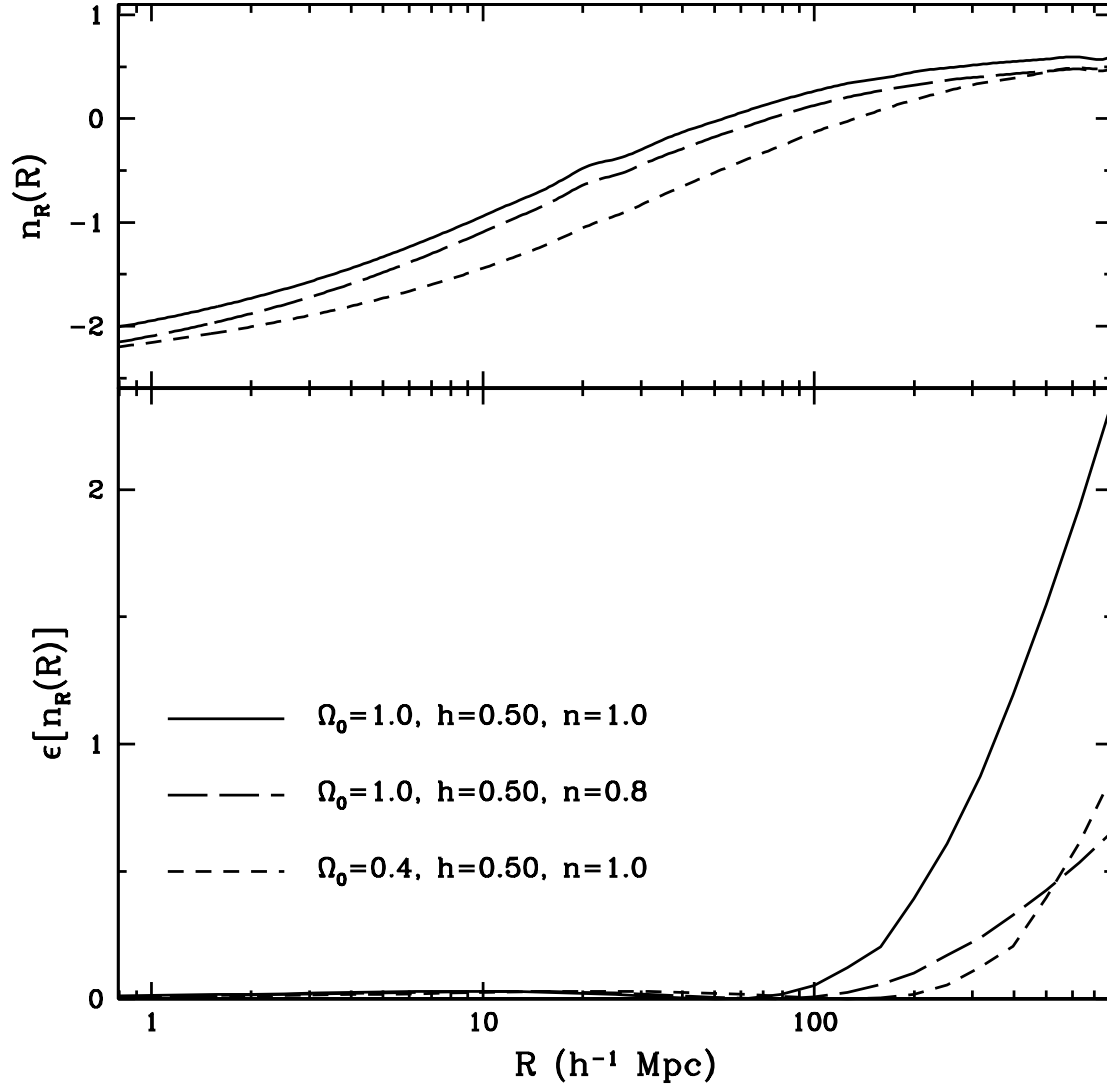


Fig. 2.— The upper panel shows the results for $n_R(R)$ for the three cosmological models described (the low- Ω_0 result is valid for both open models and flat models with a cosmological constant). The lower panel shows the variation of the ϵ term in equation (22) with smoothing scale in these CDM models. Note that this term becomes comparable to unity on scales of a few hundred h^{-1} Mpc, where $n_R(R) > 0$. The Figure should be interpreted only qualitatively, since using $\epsilon[n_R(R)]$ in equation (22) appears to overestimate the actual contribution of the higher-order terms in the sum in equation (20) for CDM models.

the impact of the $\varepsilon(n)$ term as a function of smoothing scale for various CDM models. The upper panel of Figure 2 shows $n_R(R)$ for three flat ($\Omega_0 + \Omega_\Lambda = 1$) cosmological models: standard cold dark matter (SCDM; $\Omega_0 = 1$, $h = 0.5$, $n = 1$), a tilted CDM model (TCDM; $\Omega_0 = 1$, $h = 0.5$, $n = 0.8$), and CDM with a cosmological constant (Λ CDM; $\Omega_0 = 0.4$, $h = 0.5$, $n = 1$), while the lower panel shows $\varepsilon[n_R(R)]$ for these models. One can see from equations (12), (23), and (25) that the results from the Λ CDM model will be identical to those for an open CDM model with the same value of Ω_0 (OCDM; $\Omega_0 = 0.4$, $h = 0.5$, $n = 1$). Though it appears that using n_R in the ε term in equation (22), with our nonlinear-bias model, is not strictly correct for scale-dependent power spectra (see Figure 5), we can at least qualitatively infer from Figure 2 that the contribution of the ε term to S_3 can become significant on scales $R \gtrsim 100 h^{-1}$ Mpc, particularly for models with higher values of Γ . Thus, when considering data on the moments of counts in cells, smoothed on these scales, this correction term must be included to properly account for the presence of nonlinear bias. BKJ obtain a similar correction to the angular skewness, and corresponding corrective terms should arise in leading-order perturbative calculation of higher-order moments, such as the kurtosis, S_4 , and so on. For smoothed bias, as defined in equation (24), this result implies that if $b_1^{(s)}$ and $b_2^{(s)}$ are defined at some smoothing radius R_1 , then at a sufficiently large scale $R_2 \neq R_1$, $b_2^{(s)}$ will acquire a different value due to the ε induced by the change in R . For a given CDM model, measurements of S_3 using different smoothing radii should thus yield identical results for $b_1 = b_1^{(s)}$ and b_2 , but different results for $b_2^{(s)}$.⁸ This suggests that the linear and nonlinear bias terms may be distinguishable, in a model-dependent fashion, on the basis of skewness measurements alone, provided however, that S_3 can be measured over scales sufficiently larger than $100 h^{-1}$ Mpc. An illustration of this point is shown below, in Figure 5. If, however, measurements do not show any disagreement between b_2 and $b_2^{(s)}$ on large scales, this would provide evidence to support scenarios such as peak-biasing or halo-biasing models and argue against biasing as defined in equation (3).

Since there is no known method of obtaining analytic results for the general case of the full 3PCF, assuming scale-dependent CDM power spectra, we will hereafter, for consistency, only present results obtained by numerical integration, unless otherwise noted. Many of the integrals throughout this paper involve highly oscillatory integrands, making them difficult to evaluate. We have checked that our numerical results for S_3 in particular agree to high precision with those obtained using Bernardeau’s (1994a) analytic prescription, and that our results in general are reliable to within a few percent. Figure 3 displays our numerical results for $S_3(R)$ for an unbiased ($b_1 = 1$, $b_2 = 0$) tracer-mass population in four

⁸We thank Roman Scoccimarro for clarification of this point.

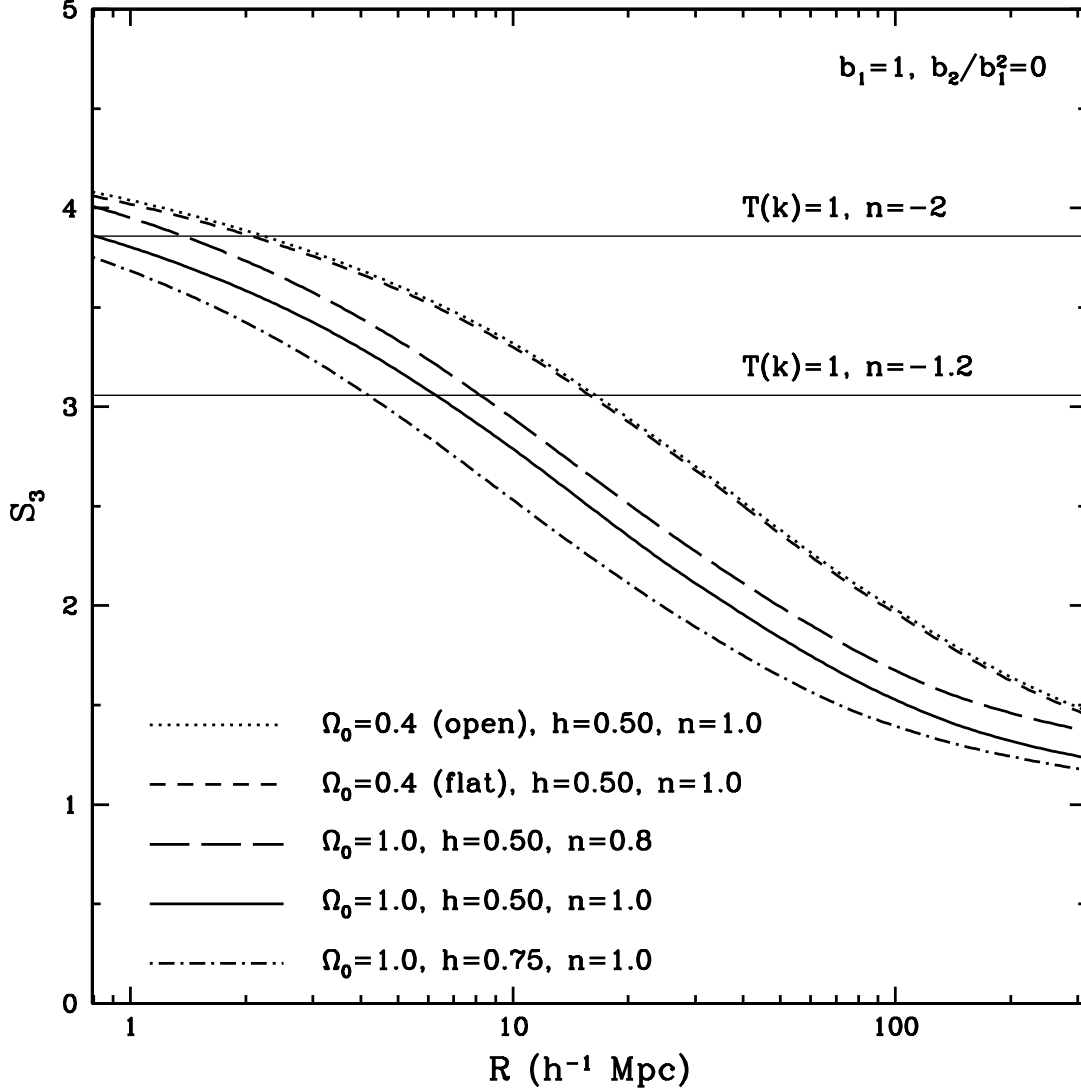


Fig. 3.— The predicted normalized skewness, $S_3(R)$, for an unbiased tracer-mass distribution smoothed with a spherical top-hat filter of radius R , for the four flat and one open cosmological models described in the text. The scale dependence of S_3 arises from the adopted CDM transfer function. By comparison, the thin horizontal lines are the results obtained using power-law spectra with $n = -2$ and $n = -1.2$. Note that the dependence of S_3 on the assumed cosmological model is fairly weak, particularly if the observed constraint, $0.2 < \Omega_0 h < 0.3$, is imposed.

flat ($\Omega_0 + \Omega_\Lambda = 1$) cosmological models: SCDM, TCDM, Λ CDM (each from above), and CDM with a high Hubble parameter (HCDM; $\Omega_0 = 1$, $h = 0.75$, $n = 1$), as well as the open CDM model (OCDM, from above).

As expected, Figure 3 shows that the CDM power spectra introduce a dependence on the smoothing scale, R , and [compared to equation (22)] a more substantial dependence on the combination of cosmological parameters in Γ . Still, the different cosmological models represented, though spanning a fairly broad range, yield fairly similar results for S_3 , certainly all consistent within the typical errors of current observations (e.g., Gaztañaga 1992; Jing & Börner 1998). The slight variation seen is due primarily to the dependence on Γ ; there is little difference between the SCDM and TCDM models (which differ only in the value of n) and virtually no difference between the OCDM and Λ CDM models, as expected from the very weak μ dependence. If the analysis is restricted to the range $0.2 < \Gamma < 0.3$, as suggested by current data (e.g., Bartlett et al. 1998), one can infer from the Figure that the predicted values for S_3 are relatively insensitive to the adopted cosmological model. In the $R \rightarrow 0$ limit, the untilted ($n = 1$) CDM curves tend toward the expected value of $(34/7) = (34/7) - (3 + n_k)$ obtained with $n_k \equiv [d \log P(k)]/d \log k = -3$, the value of the effective spectral index of the (untilted) linear-theory CDM power spectrum at small scales; for tilted models, S_3 tends toward a value $n_k - 1$ smaller. At large R , they tend toward $(6/7) = (34/7) - (3 + n_k)$, where $n_k = 1$. These perturbative results are expected to be valid at scales $R \gtrsim 5 - 10 h^{-1}$ Mpc, although as mentioned above, there are reasons to expect them to be reliable even at smaller scales. In practice, a comparison of these predictions with data will be limited at small scales by increasingly significant nonlinear effects, as well as Poisson shot noise arising from the discreteness of the counts-in-cells (Peebles 1980, Gaztañaga 1994), and at very large scales by sampling noise arising from small number of independent cells on the sky. Note for comparison, that the thin horizontal lines, which show the (virtually Ω_0 -independent) analytic results for scale-free power spectra with $n = -2$ and $n = -1.2$ [the canonical index value obtained from measurements of the 2PCF at small scales (Peebles 1980)], provide poor fits to the CDM predictions.

2.2. Effects of Bias and its Evolution

The calculations above can be generalized by allowing the bias parameters to evolve with time, as advocated by theory and observations. Peacock (1997) predicts that the linear galaxy-mass bias term evolves from a value of roughly 6 at a galaxy-formation redshift of $z_f \simeq 6 - 8$, to a nearly unbiased value of $\gtrsim 1$ today, with all models of structure formation requiring some degree of bias at $z \gtrsim 3$. Matarrese et al. (1997) explore several different

models of bias evolution, and also find that the bias for objects of between 10^{10} and 10^{13} M_\odot evolves from a value of a few at $z \simeq 5$ to roughly unity today. Studies of the clustering strength of tracer populations that span an adequately large range of redshifts, such as radio galaxies and Lyman-break galaxies, show evidence for a large bias at high redshift, which decreases with time in a manner consistent with the predictions above. (Steidel et al. 1998; Cress & Kamionkowski 1998). Assuming that objects form at a fixed redshift z_f by some arbitrary local process which induces a bias at that epoch, and are subsequently governed purely by gravity, Fry (1996) derives the result for the bispectrum of a tracer population in an Einstein-de Sitter universe, including the time-dependence of the bias parameters. Matarrese et al. (1997), refer to this as the “object-conserving” model, since it does not account for merging (see below). Tegmark & Peebles (1998) generalize the Fry model to the case where the dimensionless mass-galaxy correlation coefficient may be different than unity, but we take the Fry model as a reasonable starting point for the exploration of the effects of bias evolution.

It is straightforward to generalize the bias-evolution model of Fry (1996) to an arbitrary expansion history. Doing so, we obtain for the bispectrum in these models,

$$B(k_1, k_2, k_3, t) = P(k_1, t)P(k_2, t) \left[C_1(t) + C_2(t) \cos \theta \left(\frac{k_1}{k_2} + \frac{k_2}{k_1} \right) + C_3(t) \cos^2 \theta \right] \\ + 2 \text{ permutations,} \quad (26)$$

where

$$C_1(t) = \frac{(10/7)d^2(t) + 2(b_{1*} - 1)[d(t) - 2/7] + b_{2*}}{[d(t) + b_{1*} - 1]^2}, \quad (27)$$

$$C_2(t) = \frac{d(t)}{d(t) + b_{1*} - 1}, \quad (28)$$

$$C_3(t) = \frac{(4/7)[d^2(t) + b_{1*} - 1]}{[d(t) + b_{1*} - 1]^2}, \quad (29)$$

$d(t) = D(t)/D(t_*)$, and a subscripted asterisk denotes the value of that parameter at the epoch of formation. Note that we have now ignored the very weak dependence of the bispectrum on μ ; the dependence on the expansion history, i.e., on the species contributing to the total energy density, is contained in the growth factor, $D(t)$.

In this model, the linear-bias term effectively evolves as

$$b_1(t) = \frac{d(t) + b_{1*} - 1}{d(t)}, \quad (30)$$

decaying towards unity, as in most bias models, as the observed matter settles into the potential wells of the underlying distribution. We note that if, in reality, merging of the

tracer-mass population does in fact play a considerable role, this could result in an anti-bias ($b_1 < 1$). Anti-bias has been seen in some N -body simulations (Jenkins et al. 1997), and certain models of structure formation do require some degree of anti-bias to reconcile with current observations. The above model for bias evolution, however, will never yield $b_1(t) < 1$ if $b_{1*} > 1$. To explore this possibility, one might wish to employ other bias-evolution models which account for merging. Here, however, we are interested primarily in the qualitative dependence of the results on the dominant form of bias variation, namely, its decay with time from initially large values at high redshift.

The Einstein-de Sitter result for S_3 with bias evolution, assuming a scale-free $P(k) \propto k^n$ is presented in Fry (1996). For arbitrary $E(z)$, the result becomes

$$S_3 = \frac{d^2(t)(34/7) + (b_{1*} - 1)[6d(t) - 8/7] + 3b_{2*}}{[d(t) + b_{1*} - 1]^2} - (3 + n) \frac{d(t)}{d(t) + b_{1*} - 1}. \quad (31)$$

Here, we extend the calculation to the case of true, scale-dependent CDM power spectra, by using the bispectrum of equation (26) in (17), which amounts to making the substitutions

$$\frac{1}{b_1} \longrightarrow C_2(t), \quad \frac{1 - \mu}{b_1} \longrightarrow C_3(t), \quad \frac{b_2}{b_1^2} \longrightarrow C_1(t) - 2C_2(t) + C_3(t), \quad (32)$$

in equation (20).

Figure 4 displays the results for five different bias scenarios, each employing the SCDM, Λ CDM, and OCDM models above: an unbiased scenario ($b_1 = 1$, $b_2/b_1^2 = 0$, taken from Figure 2), a non-evolving, linear bias ($b_1 = 2$, $b_2/b_1^2 = 0$), a non-evolving, nonlinear bias ($b_1 = 2$, $b_2/b_1^2 = 1$), an evolving, linear bias ($b_{1*} = 5$, $b_{2*}/b_{1*}^2 = 0$), and an evolving, nonlinear bias ($b_{1*} = 5$, $b_{2*}/b_{1*}^2 = 1$). For the non-evolving bias scenarios, the Λ CDM and OCDM models are taken to be identical, as suggested by Figure 2. These models do, however, differ in the case of evolving bias due to the different time dependence of the linear growth factor, and the differences between them would increase with decreasing Ω_0 . For the evolving cases we assume a formation redshift of $z_f = 5$. In calculating the expressions involving b_2 , we must evaluate sums of the kind in equation (20). Numerical tests show that these converge rapidly, typically requiring at most three terms to achieve percent-level accuracy.

These models are intended as an illustrative, but by no means exhaustive, representation of the possibilities. Even so, it is clear from Figure 4 that that $S_3(R)$ depends far more sensitively on the overall form of the bias than on the values of Γ or Ω_0 within an individual biasing scheme. For example, adding a very slight linear bias to the low- Γ model would yield a result similar to the unbiased SCDM prediction, within current error estimates. Generally, the presence of any significant linear bias, $b_1 > 1$, flattens the $S_3(R)$ curve, as compared with the unbiased case (solid lines). Furthermore, an observed $S_3(R)$ curve which

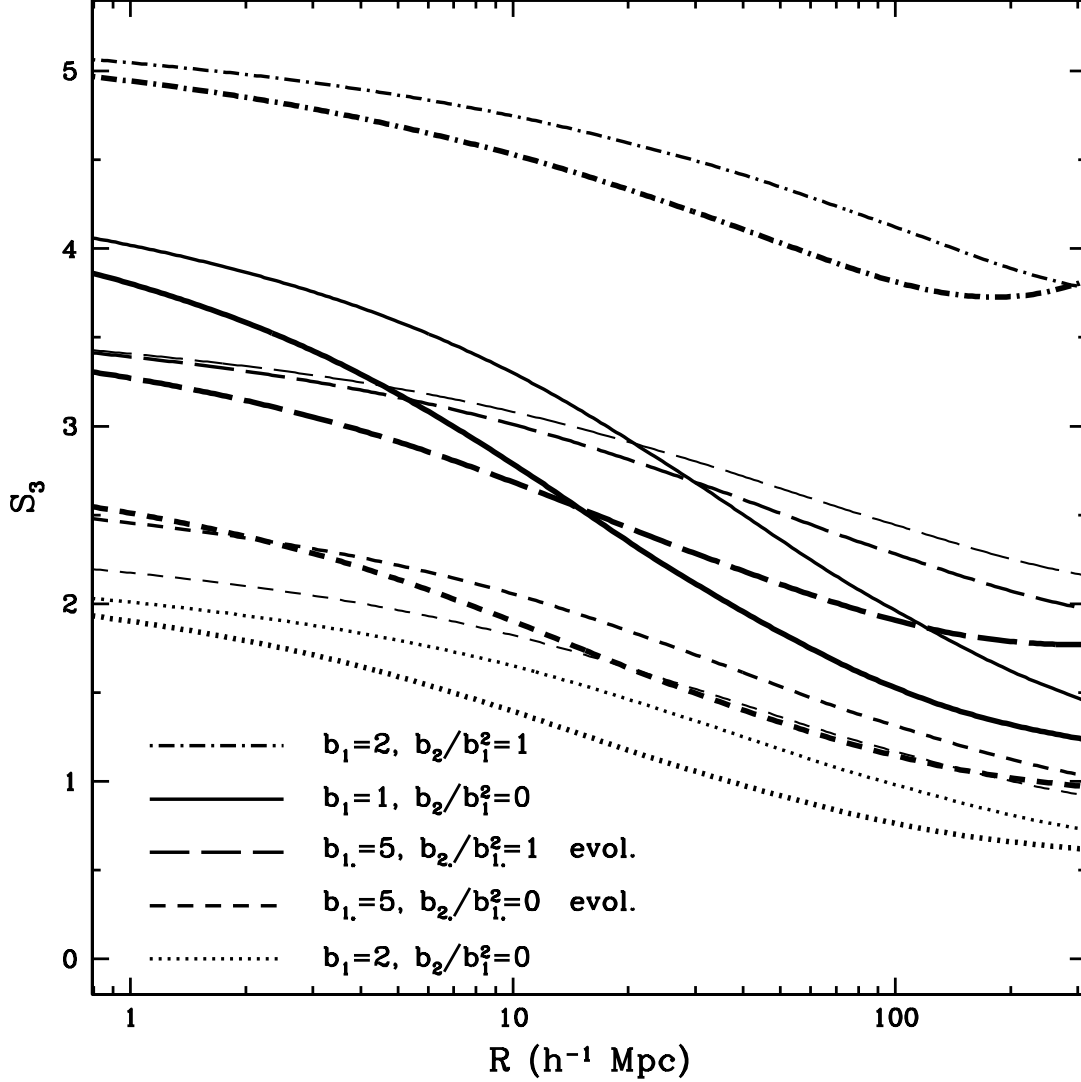


Fig. 4.— The predicted normalized skewness for the five different bias scenarios described in the text. For each case, the SCDM, Λ CDM, and OCDM models are shown in thick, medium, and thin lines, respectively (for the non-evolving bias scenarios, the latter two models are identical). Note that the dependence on the overall biasing scheme far outweighs that on the cosmological parameters within a given scheme. In particular, a linear (nonlinear) bias term lowers (raises) the predicted curve with respect to the unbiased case, and a significant linear bias term flattens the curve appreciably.

is well below the predicted unbiased result can only be achieved by a significant linear bias term (assuming $b_2 \geq 0$), while one well above this value can only arise from the existence of a non-zero b_2 term or from anti-biasing ($b_1 < 1$). In general, the curves for an evolving bias produce less drastic shifts than their non-evolving counterparts, despite the fact that the respective bias terms are initially larger. This is because the evolution towards an unbiased state effectively mimics a smaller, constant bias [c.f. equation (30)]. Note that the SCDM models with nonlinear bias exhibit an upturn at large R , arising from the contribution of the higher-order terms in the sum in equation (20). The other CDM models with nonlinear bias show an upturn only at larger scales, as suggested by Figure 2.

Figure 4 also reveals that, despite the separate dependences of S_3 on b_1 , b_2 , and their evolution, different biasing scenarios may be very difficult to distinguish on the basis of the skewness measurements alone. Different sets of parameter choices could easily yield curves for the various scenarios which essentially overlap, requiring high-accuracy data to differentiate them. An example of this is shown in Figure 5, where we see that, for scales $R < 100 h^{-1}$ Mpc, the results from an SCDM model with constant, nonlinear bias, an OCDM model with evolving, linear bias, and an OCDM/ Λ CDM model with constant, linear bias, are very similar. The OCDM model with evolving, linear bias is taken from Figure 4, and according to equation (30), is expected to be similar to an open model with a constant value of $b_1 = 2.04$, or a Λ CDM model with a constant $b_1 = 1.8$, and indeed Figure 5 shows this to be the case. For an inferior data set, this degeneracy between the cosmological parameters, and in particular b_1 , b_2 , and their time dependence, cannot be broken with the skewness, measured on scales $R < 100 h^{-1}$ Mpc, as it provides only one constraint on the combination of these quantities. Note, however, that for $R \gtrsim 100 h^{-1}$ Mpc, the SCDM model with nonlinear bias can be better distinguished due to the different scale dependence arising from the higher-order terms in the sum in equation (20). For comparison, the thin dot-dashed line shows the same result obtained using $\varepsilon[n_R(R)]$ in equation (22), which appears to overestimate the numerical result (thick lines) obtained by evaluating the the sum in equation (20). If this large-scale variation induced by nonlinear biasing is observed, it would allow better constraints on both the linear and nonlinear bias parameters solely from measurements of S_3 . The absence of this behavior would still provide valuable insight, arguing against our bias model and in favor of smoothed-bias models, where b_1 and b_2 tend towards constants at large scales. However, it is at present unlikely that S_3 could be measured on such large scales with sufficient precision to address these issues.

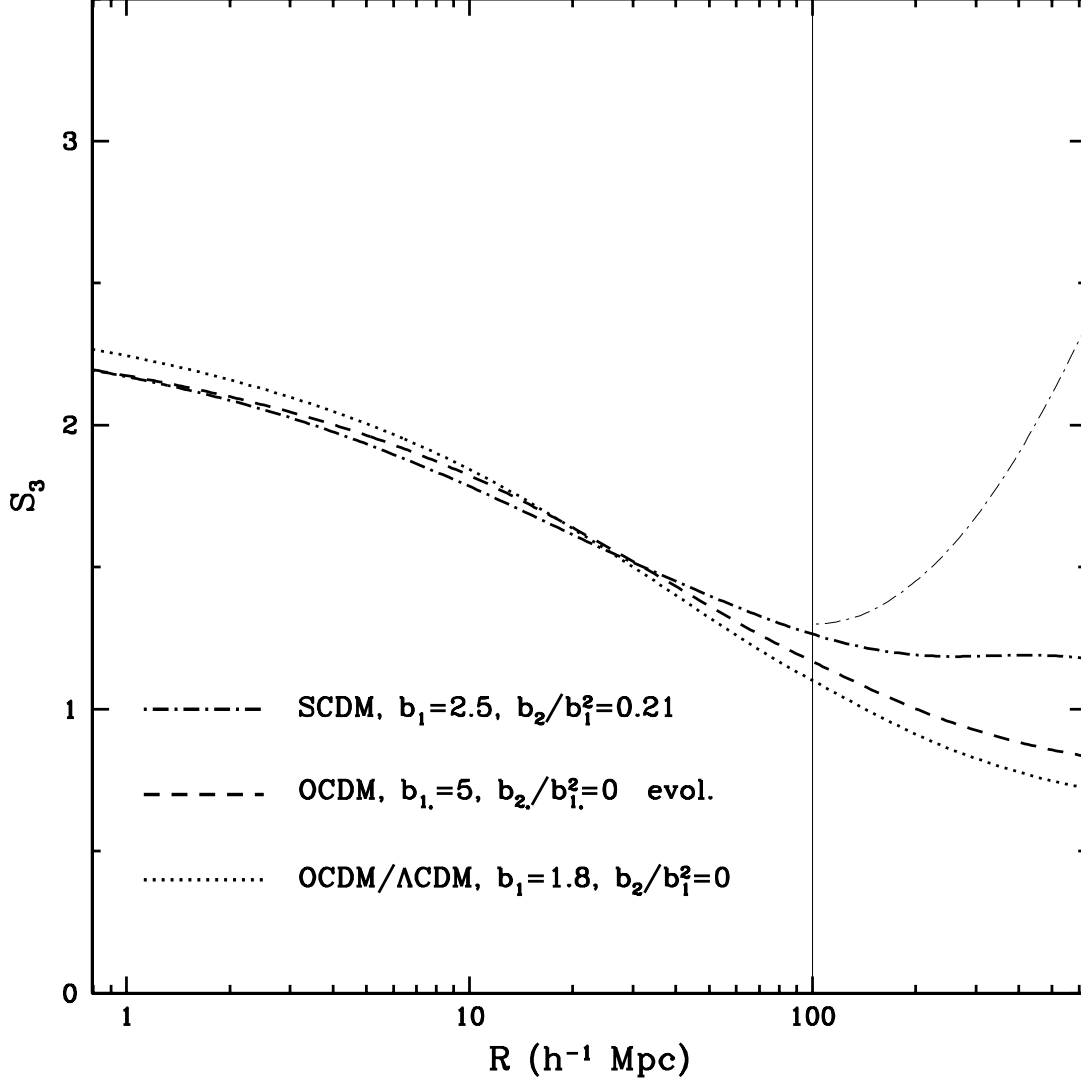


Fig. 5.— An example of nearly degenerate predictions for $S_3(R)$, arising from the fact that the skewness provides only one constraint on the combination of the cosmological and bias parameters, and the evolution of the latter. In this case, the SCDM model with constant nonlinear bias, OCDM model with evolving linear bias, and OCDM/ Λ CDM model with constant linear bias are nearly identical out to smoothing scales of $R \simeq 100 h^{-1} \text{ Mpc}$. Above this scale, the SCDM model with nonlinear bias can be better distinguished due to the different scale dependence introduced by higher-order terms in the sum in equation (20). For comparison, the thin dot-dashed line shows the SCDM result using equation (22) with $\varepsilon[n_R(R)]$, and appears to overestimate the impact of the nonlinear term at large scales.

3. SPATIAL THREE-POINT CORRELATION FUNCTION

The one-point statistic S_3 , is a volume-averaged quantity and thus, while it is seen to preserve information about the overall dependence of clustering strength with scale, discards detailed information about the configuration dependence contained in the full 3PCF. It has been shown, for example, that the configuration dependence of the bispectrum and 3PCF in leading-order PT can be used to separate the contributions of gravitational clustering and bias to the observed power (FG93; Fry 1994; Frieman & Gaztañaga 1994), as well as obtain multiple, independent constraints on the combination of the constant b_1 and b_2 parameters (Jing & Zhang 1989; Gaztañaga & Frieman 1994; Fry 1994, 1996; Jing 1997; Matarrese, Verde, & Heavens 1997).

Much attention has therefore been focused on the normalized spatial 3PCF,

$$Q(r_{12}, r_{23}, r_{31}) = \frac{\zeta(r_{12}, r_{23}, r_{31})}{\xi(r_{12})\xi(r_{23}) + \xi(r_{12})\xi(r_{31}) + \xi(r_{23})\xi(r_{31})}, \quad (33)$$

where the lengths r_{ij} form a triangle in real space. We can evaluate this expression using equations (5) and (13), where we no longer include the window functions since we presume that the CFs are obtained from direct counting, rather than from smoothed counts in cells. In this case, it is more natural to use the unsmoothed bias parameters defined by equation (3), rather than the smoothed bias parameters of equation (24). Using the techniques and conventions of the previous sections, we obtain, after some manipulations, the spatial 2PCF,⁹

$$\xi(r) = \frac{1}{2\pi^2} \int dk k^2 P(k) \frac{\sin kr}{kr} = \frac{Ab_1^2 D^2(t)}{2\pi^2 r^{n+3}} \int dx x^{n+2} T^2(x/r) \frac{\sin x}{x}, \quad (34)$$

and 3PCF,

$$\zeta(r_{12}, r_{23}, r_{31}) = \frac{A^2 b_1^4 D^4(t)}{4\pi^4} \frac{1}{r_{31}^{n+3} r_{23}^{n+3}} \int_0^\infty dx_1 x_1^{n+2} T^2(x_1/r_{31}) \int_0^\infty dx_2 x_2^{n+2} T^2(x_2/r_{23})$$

⁹Had we wished to calculate the 2PCF using counts in cells, there would be an additional factor of $W^2(xR/r)$ in the integrand, and corresponding terms in the 3PCF, which would alter the results on scales where R/r is non-negligible (i.e., separations comparable to the cell size), to account for the effects of smoothing on correlations at these scales. The dependence of the CFs on the ratio between the smoothing half-width and the pair separation can be appreciable; for scale-free power spectra with $n = -2.2, -1.2, -0.2, 0.8$ this term adds corrections to ξ of 1%, 10%, 49%, and 294% for $r = 2R$, dropping to 0.14%, 1.2%, 4.3%, and 2.9% for $r = 5R$. For a CDM power spectrum, with $\Gamma = 0.5$, the corrections are more significant: 42%, 11%, and 2.4% for r/R values of 2, 5, and 10, respectively. For counts-in-cells CFs, one must take care to restrict measurements to scales significantly larger than the smoothing radius, or include the smoothing terms in the theoretical calculations.

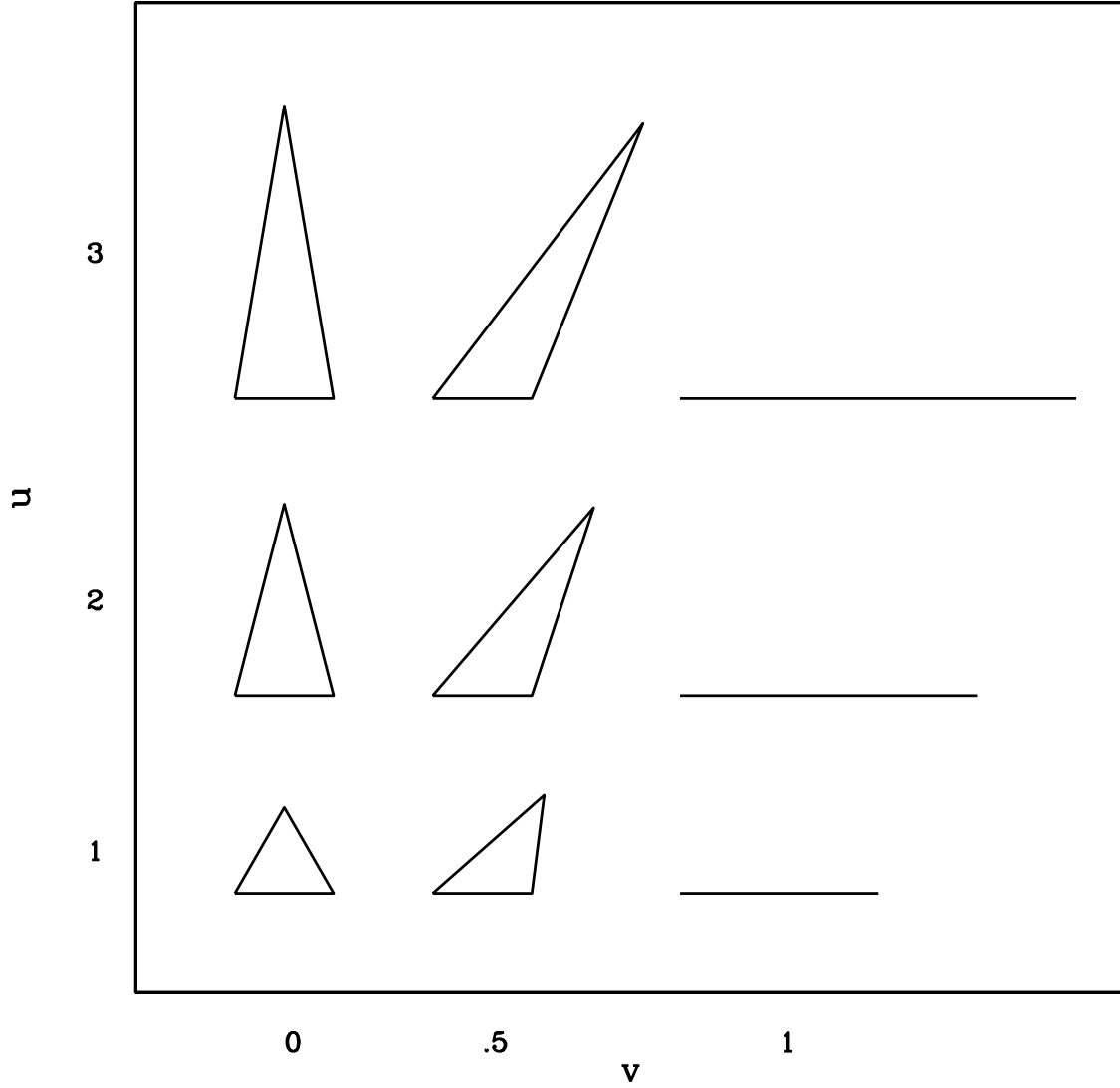


Fig. 6.— The variation of triangle geometry with u and v , for a fixed value of r given by the side of the $u = 1$, $v = 0$ equilateral triangle. Triangles with $u = 1$ are isosceles with the shorter sides equal, those with $v = 0$ are isosceles with the longer sides equal, and $v = 1$ yields a colinear configuration. Larger values of u and/or v pick out more elongated structures.

$$\begin{aligned}
& \times \left\{ \left(\frac{1+\mu}{b_1} + \frac{b_2}{b_1^2} \right) \frac{\sin x_1}{x_1} \frac{\sin x_2}{x_2} \right. \\
& - \frac{1}{b_1} \cos \theta_{12} \left(\frac{r_{23}}{r_{31}} x_1^2 V(x_1) V(x_2) + \frac{r_{31}}{r_{23}} x_2^2 V(x_1) V(x_2) \right) \\
& + \frac{1-\mu}{b_1} \left[\cos^2 \theta_{12} Y(x_1) Y(x_2) + 3V(x_1) V(x_2) \right. \\
& \left. \left. - Y(x_1) V(x_2) - Y(x_2) V(x_1) \right] \right\} + (\text{cyc.}), \tag{35}
\end{aligned}$$

where $\cos \theta_{12}$ is the angle between \mathbf{r}_{13} and \mathbf{r}_{23} , $V(x) = W(x)/3$, and $Y(x) \equiv W(x) - (\sin x)/x$. For an evolving bias, we simply change

$$\left(\frac{1+\mu}{b_1} + \frac{b_2}{b_1^2} \right) \longrightarrow C_1(t), \quad \frac{1}{b_1} \longrightarrow C_2(t), \quad \frac{1-\mu}{b_1} \longrightarrow C_3(t). \tag{36}$$

Equation (35) does not contain terms analogous to the higher-order terms in the sum in equation (20) [or to the $\varepsilon(n)$ term in equation (22)], since evaluation of the 3PCF by direct counting requires no smoothing. With our bias model, such terms would be induced, however, from the calculation of the 3PCF using counts in cells (see footnote). One must be careful to realize that the nonlinear-bias parameter measured from the direct-counting 3PCF in equation (35) will be different from the smoothed value inferred from the FG93 result for S_3 (or, equivalently, from that inferred from the counts-in-cells 3PCF), though the two can be related, e.g., via the $\varepsilon(n)$ term in equation (22).

The dependence of $\xi(r)$ on $r^{-(n+3)}$ in the prefactor of equation (34) is the familiar result, yielding $\xi(r) \propto r^{-1.8}$ for a scale-free power spectrum with the canonical value of $n = -1.2$ (Peebles 1980). For more realistic CDM power spectra, there is an additional dependence on r arising from the scale dependence of the transfer function. Similarly, had we ignored the shape-dependent terms in the bispectrum [equation (15)], we would arrive at the standard empirical “approximation” for the 3PCF, $\zeta(r_{12}, r_{23}, r_{31}) \propto \xi(r_{12})\xi(r_{23}) + \xi(r_{12})\xi(r_{31}) + \xi(r_{23})\xi(r_{31})$. However, the true scale and shape dependences of the 3PCF, as manifested in equation (35), can be exploited to gain far more information (Fry 1984; Jing & Börner 1997). Following Peebles & Groth (1975), we take

$$r = r_{12}, \quad u = \frac{r_{23}}{r_{12}}, \quad v = \frac{r_{31} - r_{23}}{r_{12}} \tag{37}$$

as the defining parameters for a triangle, where $r_{12} < r_{23} < r_{31}$, so that $u \geq 1$ and $0 \leq v \leq 1$. For this convenient choice of parameters, r fixes the overall size of the triangle, while u and v determine the exact size and shape. Figure 6 shows the variation of the geometry with u and v for a given choice of r .

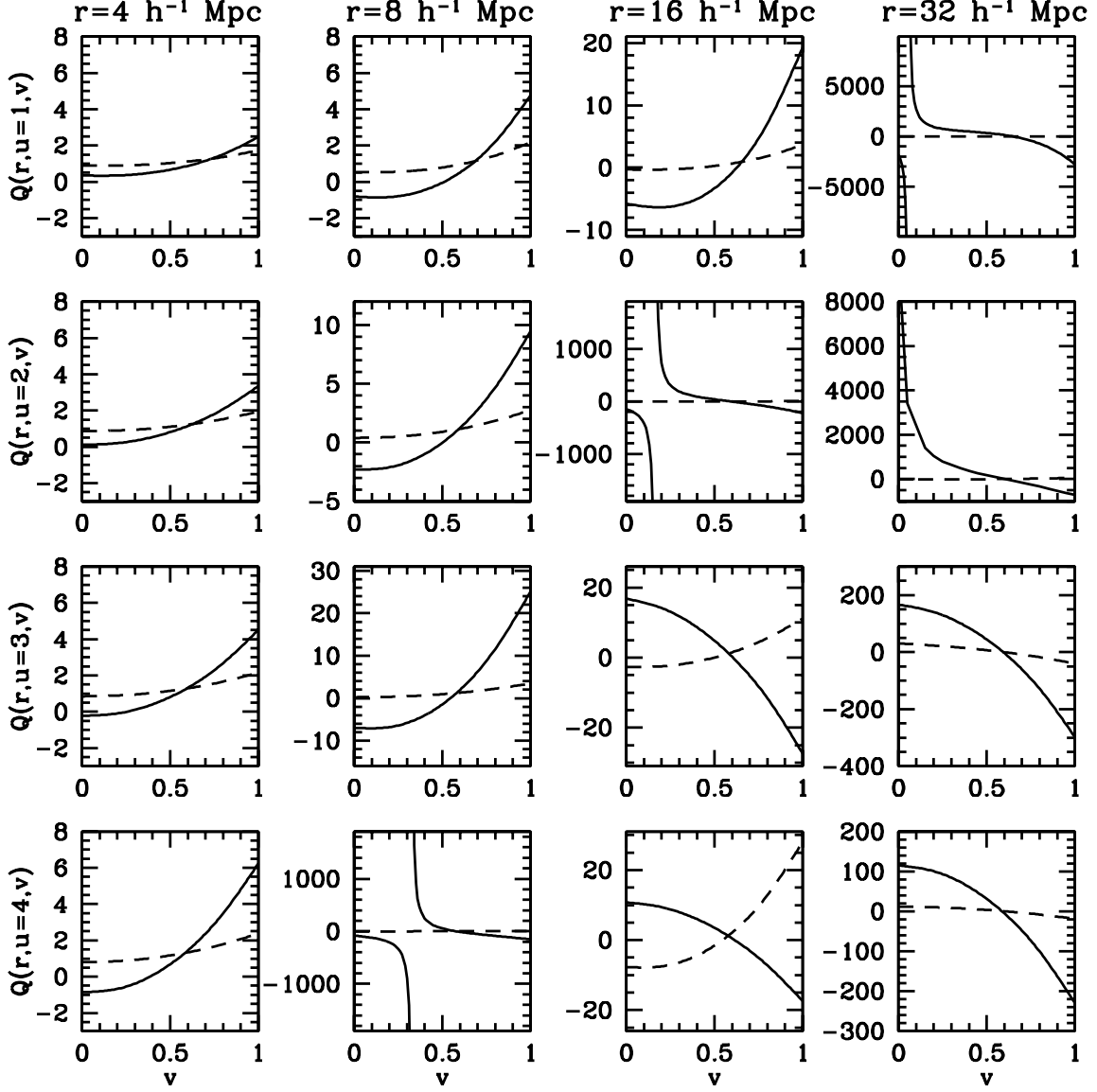


Fig. 7.— Predicted normalized 3PCF, $Q(r, u, v)$, for the $\Gamma = 0.5$ (SCDM, solid lines) and $\Gamma = 0.2$ (OCDM/ACDM, dashed lines) models without bias. The columns represent values of $r = 4, 8, 16, \text{ and } 32 \ h^{-1} \text{ Mpc}$ (left to right) while the rows represent values of $u = 1, 2, 3, \text{ and } 4$ (top to bottom). Note the different scalings on the vertical axes. Over these scales, the SCDM model shows dramatic variation of Q with triangle geometry, exhibiting divergences in some cases.

3.1. Results with no Biasing

3.1.1. The Problem With Q

Figure 7 shows the normalized spatial 3PCF, Q , plotted as a function of r , u , and v , using the transfer function of equation (21) for the $\Gamma = 0.5$ (SCDM) and $\Gamma = 0.2$ (OCDM/ Λ CDM) models, assuming no bias. The weak μ dependence makes the OCDM and Λ CDM models nearly indistinguishable on the scale of Figure 7, so only the former is plotted. Note the different scalings and the dramatic, non-monotonic variation and divergences seen for certain configurations, particularly in the SCDM model. JB97 also derive QL PT predictions for Q in CDM models and find very similar results for its configuration dependence, though they do not show cases where the behavior is particularly egregious. Comparing these results with those from N -body simulations, however, JB97 and Matsubara & Suto (1994) find that the predicted differences between various CDM models in N -body simulations are markedly less than those predicted by QL PT, and moreover that in simulations, these models in general show far less rapid variation of Q with geometry than is seen in the QL PT predictions. JB97 claim that this discrepancy is due primarily to the absence of nonlinear corrections in the PT calculation, but we suggest another possibility. In the top panel of Figure 8 we show our prediction for $Q(v)$ in a $\Gamma = 0.5$ model for $r = 8 h^{-1}$ Mpc and $u = 4$. The lower panel reveals that the divergence in Q is caused not by any irregular behavior of ζ (which is seen to vary in a smooth, monotonic fashion), but rather by the behavior of the denominator in equation (33), which vanishes in this case at $v \simeq 0.325$ (note that we have multiplied the numerator and denominator of equation (33) by 10^{10} and 10^{12} , respectively, for clarity). In this sense, Q is a poorly defined quantity, whose variation may not reflect any rapid variations in ζ , but rather stems from the manner in which ζ is normalized. For the cases shown in Figure 7, Q is particularly rapidly varying in the SCDM model only because the region of the power spectrum effectively sampled by a value of $\Gamma = 0.5$ happens to yield vanishing behavior of $\xi(r_{12})\xi(r_{23}) + \xi(r_{12})\xi(r_{31}) + \xi(r_{23})\xi(r_{31})$ for some of the chosen configurations; similar behavior would be seen in other models at appropriately different scales.

We speculate that the above-mentioned disagreement with N -body predictions, which show far less variation in Q , may simply be due to the practical inability to measure $\xi(r_{12})\xi(r_{23}) + \xi(r_{12})\xi(r_{31}) + \xi(r_{23})\xi(r_{31})$ to high precision near zero, thus smoothing out the N -body result for Q . This conclusion is supported by the fact that all previous investigations find that the QL PT predictions for S_3 , which is normalized by a positive-definite quantity

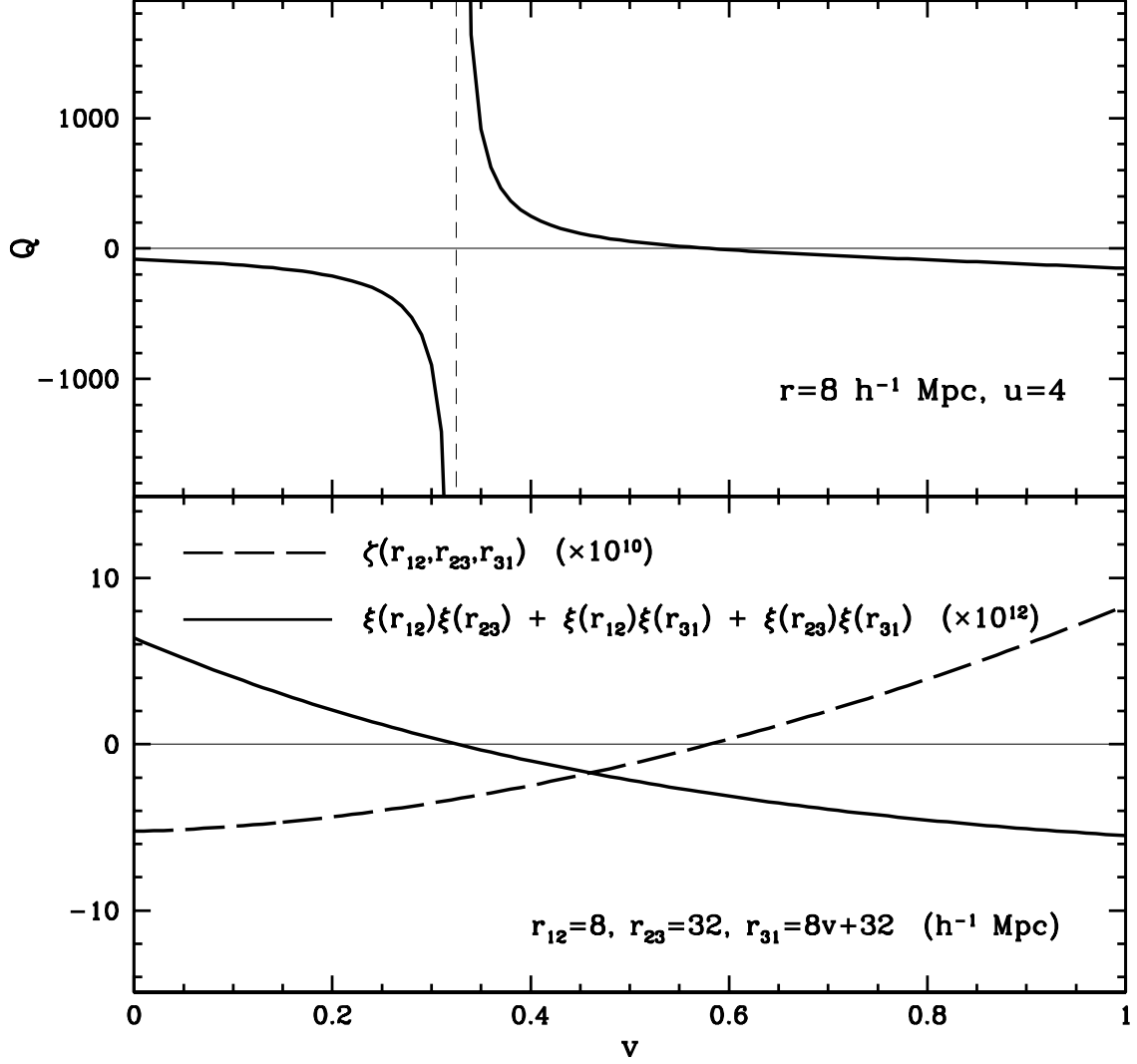


Fig. 8.— The top panel shows the predicted $Q(v)$ for $r = 8 \text{ h}^{-1} \text{ Mpc}$ and $u = 4$, while the bottom panel shows the separate behaviors of the numerator (multiplied by 10^{10} ; dashed line) and denominator (multiplied by 10^{12} ; solid line) of equation (33) for this configuration. The 3PCF itself is smoothly varying; the large values of Q arise from the small values of the denominator, which passes through zero at $v \simeq 0.325$.

(i.e., the square of the variance), *do* agree with N -body results over the scales of interest¹⁰ (Bouchet, Schaeffer, & Davis 1991; Fry, Melott, & Shandarin 1993, 1995; Bernardeau 1994a; Baugh, Gaztañaga, & Efstathiou 1995; Colombi, Bouchet, & Hernquist 1996; JB97). We propose that this explanation for the discrepancy in Q can be evaluated against the nonlinear-effects argument of JB97 by considering N -body results at earlier epochs, where nonlinearities in the distribution of fluctuations are known to be small. We point out that the Fourier-space \mathcal{Q} , defined in equation (1), is normalized by a positive-definite quantity, and does not suffer from this problem entailed in the definition of the real-space Q .

3.1.2. Results for the 3PCF

To avoid the above difficulties altogether, we define $Q_V = \zeta/[\xi_{8h^{-1}\text{Mpc}}(0)]^2$; i.e., we normalize the 3PCF (like s_3) by the square of the variance at a fixed smoothing scale, calculated for each model using equation (12). Thus, Q_V is still independent of the power-spectrum normalization, but does not exhibit the rapidly-varying or divergent behavior seen with Q , since we are now dividing by a positive-definite quantity. The adopted smoothing scale is arbitrary; $8h^{-1}\text{Mpc}$ is chosen merely for convenience.

Figure 9 illustrates our predictions for $Q_V(r, u, v)$ for the SCDM, OCDM/ Λ CDM, and TCDM models with no bias. Note that Q_V is everywhere a smoothly-varying and well-behaved function. Since, in each model, Q_V is normalized by a fixed quantity, the Figure clearly reveals the expected decrease in the 3PCF with increasing r . This behavior, however, is not simply the $r^{-2(n+3)}$ variation predicted by the hierarchical model, which also fails to produce the shape dependence of the 3PCF. In general, we see that, within a given cosmological model, Q_V increases with increasing v . Physically, this implies that clustering in the quasi-linear regime favors colinear structures (see Figure 6), which can be identified, in the early stages of structure formation, with collapsed structures such as sheets and filaments. The decrease in Q_V with increasing u is due to a combination of the scale and shape dependences; larger values of u pick out both larger and more elongated structures, giving rise to competing effects. Under our chosen normalization convention, the former effect wins out. Fry (1994, 1996) finds similar results by considering the k -space \mathcal{Q} , defined in equation (1). Though the CDM models shown all exhibit these common trends, the precise behaviors predicted for Q_V by models with different values of Γ are quite distinct, owing to the different locations of the peaks in their power spectra. Overall,

¹⁰Hui & Gaztañaga (1998) note a separate measurement bias, applicable to S_3 as well, arising from the fact that the ratio of two unbiased estimators is not unbiased estimator.

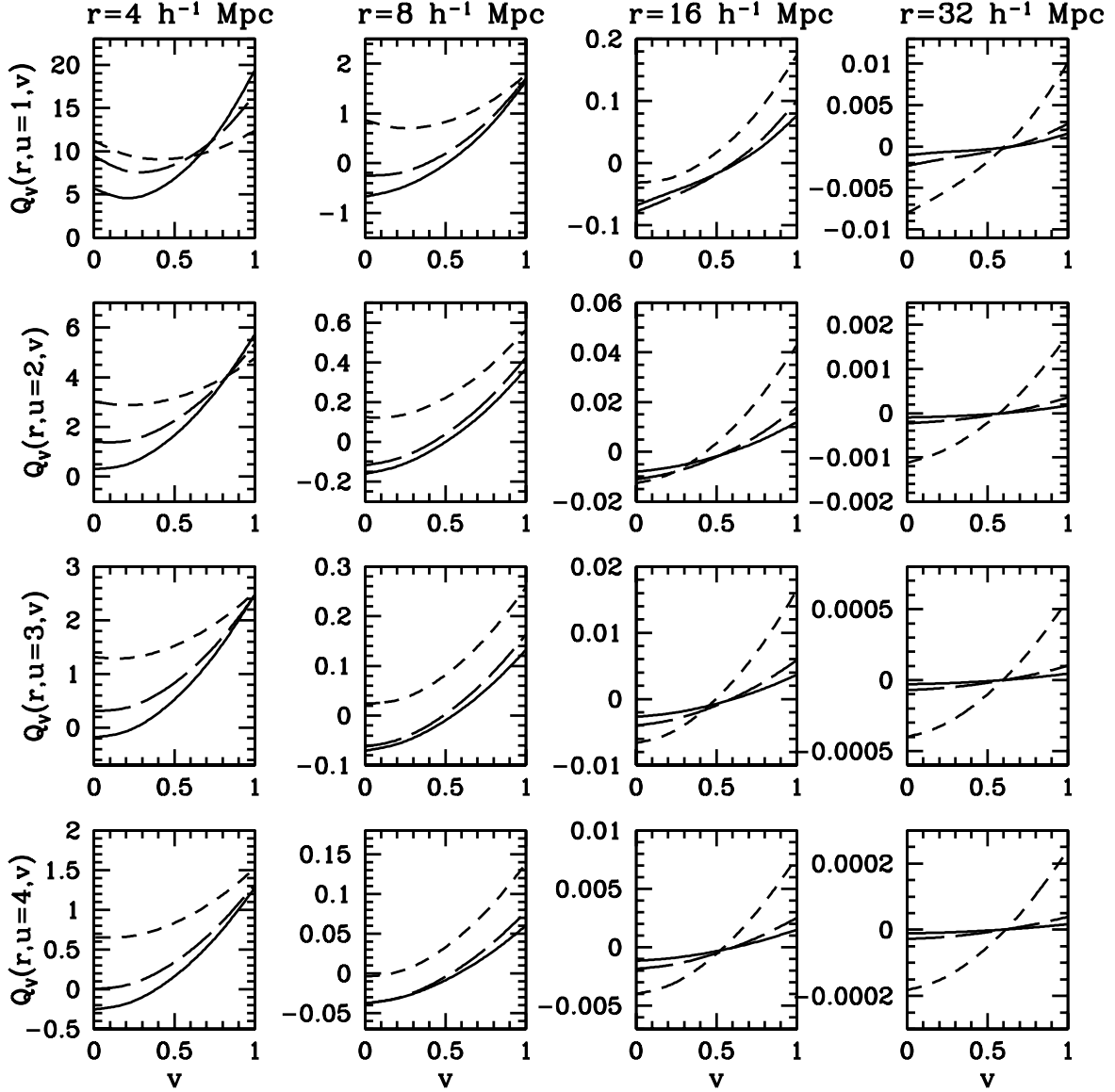


Fig. 9.— Predicted $Q_V(r, u, v)$ for the unbiased SCDM (solid lines), OCDM/ Λ CDM (short-dashed lines), and TCDM (long-dashed lines) models. The columns represent values of $r = 4, 8, 16,$ and $32 \ h^{-1} \text{ Mpc}$ (left to right) while the rows represent values of $u = 1, 2, 3,$ and 4 (top to bottom). Note the different scalings on the vertical axes. All three models indicate that clustering strength decreases with scale and increases with increasing v . Models with different values of Γ , however, yield distinct predictions for Q_V , though the SCDM and TCDM models, which differ only in the value of n , are not well distinguished on large scales.

Figure 9 suggests that measurements of the 3PCF on these scales, though not very sensitive to changes in the value of n (see BKJ), may discriminate well between high- Γ and low- Γ models.

3.2. Effects of Bias and Its Evolution

Figure 10 shows $Q_V(v)$ for the five bias scenarios from §2.2 for the OCDM and Λ CDM models (taken to be identical in the non-evolving bias cases) for $r = 8 \ h^{-1}$ Mpc and $u = 4$. This represents only a small region of the parameter space we are exploring, but we find similar dependences of the 3PCF on the bias scheme as were seen for S_3 , namely a general flattening and reduction of Q_V with increasing linear bias, and a relative increase with increasing nonlinear bias as compared with the corresponding linear scheme. In the evolving cases, the difference between these two models, which arises from their different linear growth factors, would be greater for lower values of Ω_0 .

Whereas the skewness gave only a single relationship, $S_3(R)$, with which to distinguish different cosmological and biasing schemes, the full 3PCF allows much stronger constraints from consideration of the geometric dependence [i.e., a graph such as Figure 10 for every pair of values (r, u)]. We illustrate this in Figure 11, where $Q_V(r, u, v)$ is plotted for the same three (nearly degenerate) models depicted in Figure 5. The constant linear- and nonlinear-bias schemes (dotted and dot-dashed curves, respectively), which gave nearly identical results for S_3 , yield distinct predictions for Q_V , in part because of their different values of Γ as well. It is well-known that measurements of the bispectrum and 3PCF can be used to obtain independent constraints on the constant-valued linear and nonlinear bias parameters (FG93; Fry 1994, 1996; Jing 1997; Matarrese, Verde, & Heavens 1997); this can be seen here from the different manners in which these terms appear in equation (35). The low- Γ models in Figure 11, with linear, evolving (dashed curves) and non-evolving (dashed curves) bias, however, remain fairly similar, since an initially large, evolving value of b_1 again approximates a correspondingly smaller constant term. Though the relative differences between these models are slightly more pronounced at larger scales, it is unlikely that current and emerging redshift surveys will attain sufficient precision to resolve them. Thus, while the geometric information contained in the present-day 3PCF can, unlike S_3 , be used to distinguish between different cosmological models and separate the contributions of constant linear- and nonlinear-bias terms, it may not reliably distinguish between constant and evolving bias.

This ambiguity could, in principle, be removed by considering measurements of the spatial 3PCF as a function a redshift, as might be obtained from very deep surveys. Figure

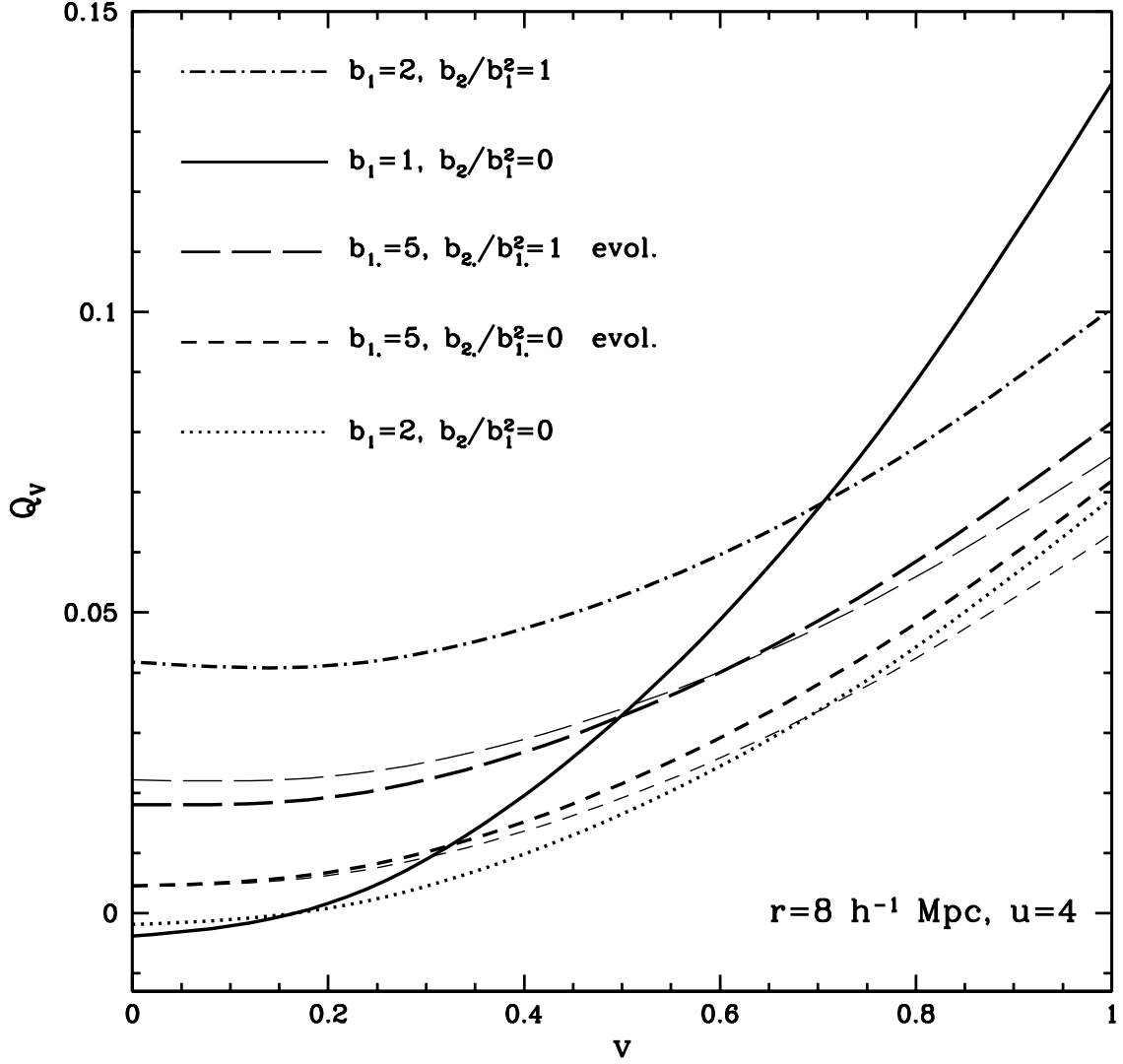


Fig. 10.— Predicted $Q_V(v)$ for $r = 8 \, h^{-1} \text{ Mpc}$ and $u = 4$ for the five bias scenarios shown. For each scenario, the Λ CDM and OCDM models are shown in thick and thin lines, respectively, with the two models being effectively identical in the non-evolving cases, but distinct in the evolving cases due to their different linear growth factors.

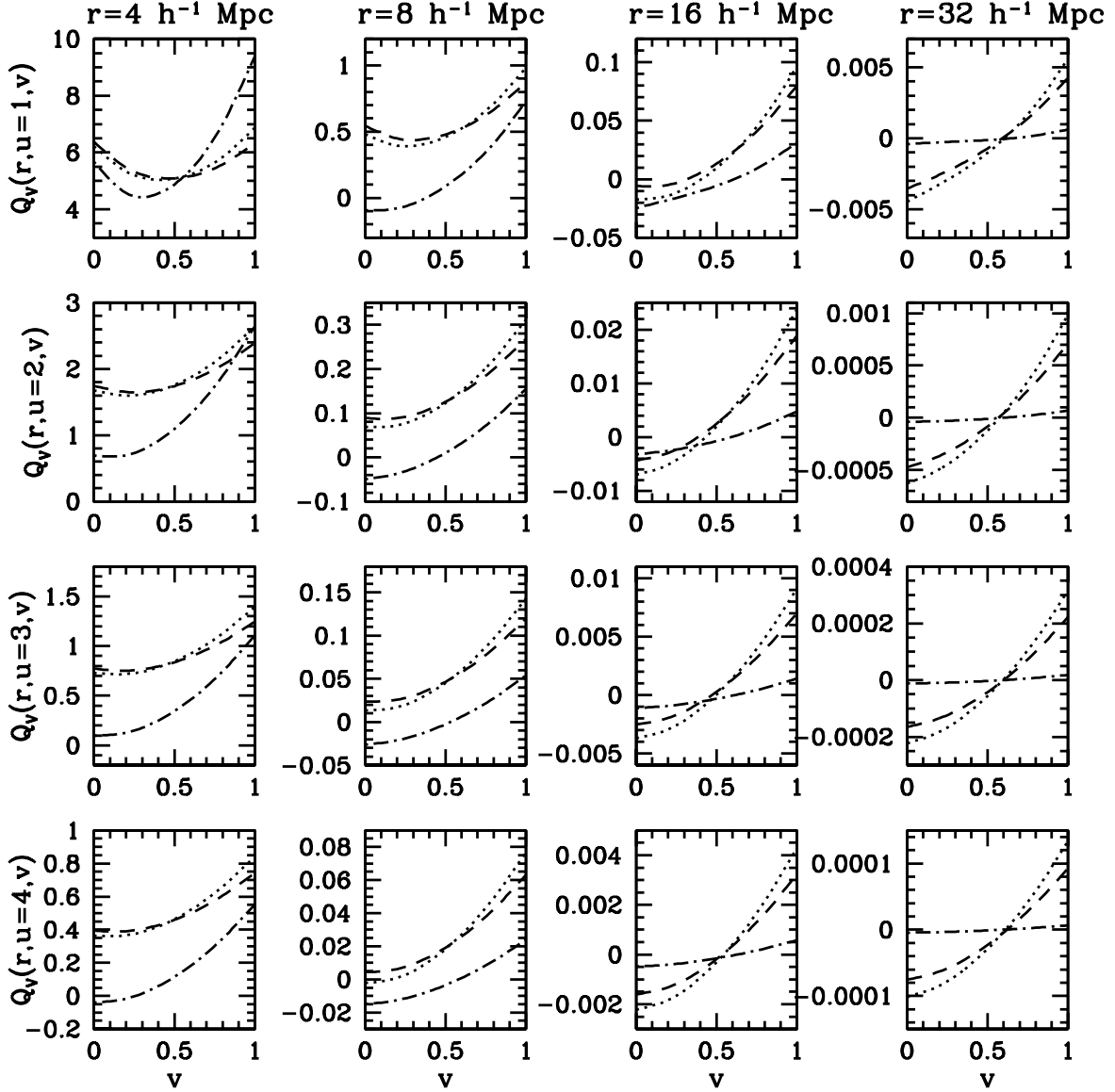


Fig. 11.— Predicted $Q_V(r, u, v)$ for the SCDM, $b_1 = 2.5$, $b_2/b_1^2 = 0.21$ model (dot-dashed curves), OCDM, $b_{1*} = 5$, $b_{2*}/b_{1*}^2 = 0$ model (dashed curves), and OCDM/ Λ CDM, $b_1 = 1.8$, $b_2/b_1^2 = 0$ model (dotted curves). The constant linear- and nonlinear- bias models (dotted and dot-dashed, respectively) yielded degenerate S_3 predictions, but can be distinguished using the full geometric dependence of Q_V (in part because of their different values of Γ). The evolving and non-evolving linear models (dashed and dotted, respectively), however, are not as well distinguished by measurements of the present-day 3PCF alone.

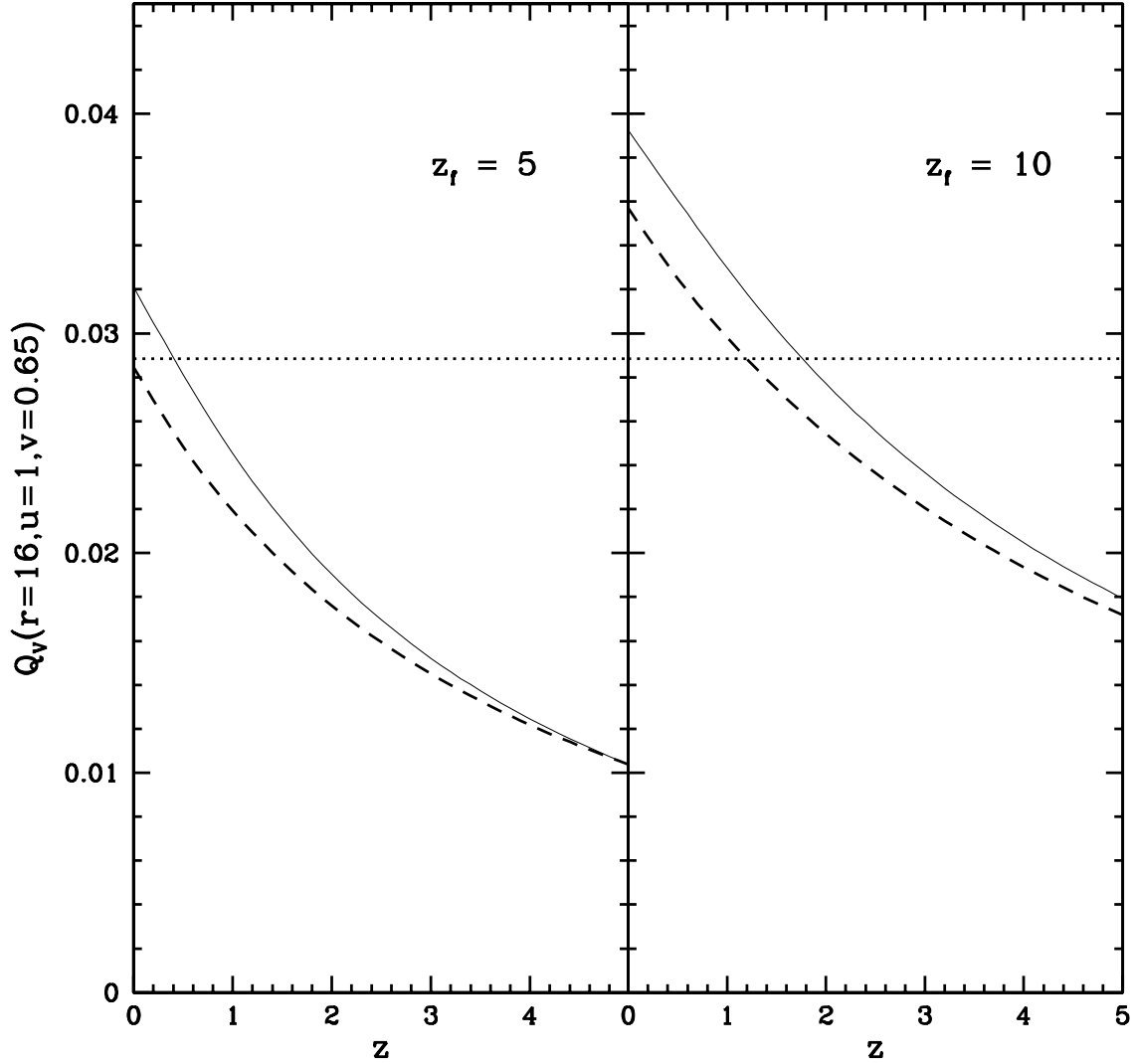


Fig. 12.— The variation of Q_V with redshift for a fixed triangle configuration ($r = 16 \ h^{-1}$ Mpc, $u = 1$, $v = 0.65$). The dotted lines show the result for the OCDM/ Λ CDM model with constant linear bias, $b_1 = 1.8$, while the dashed lines show the evolving linear bias, $b_{1*} = 5$, result for the OCDM. The evolving and constant OCDM models are virtually identical at $z = 0$, but can be distinguished by their different redshift-dependences. An evolving, Λ CDM model is shown by the thin, solid lines, for comparison. The right panel shows the results obtained using a formation redshift of $z_f = 10$, rather than $z_f = 5$.

12 shows the evolution of Q_V with redshift, for a particular configuration ($r = 16 h^{-1}$ Mpc, $u = 1$, $v = 0.65$), for the OCDM evolving linear bias model and OCDM/ Λ CDM constant linear bias model from Figures 5 and 11, with a Λ CDM evolving linear bias model added for comparison. These evolving and non-evolving cases yielded similar results for Q_V as well as S_3 , and for this particular configuration were practically identical, as can be seen in the appropriate panel of Figure 11, or from the $z = 0$ result in Figure 12. We see, however, that the constant linear bias model can be distinguished from the evolving models on the basis of their evolution with redshift. Note that, unlike the constant-bias case where the negligible dependence on μ caused the OCDM and Λ CDM predictions to differ only by the thickness of the curves, the evolving OCDM and Λ CDM models here yield different results, as expected, with the differences becoming larger for smaller values of Ω_0 . Comparing the left and right panels further illustrates the dependence on the redshift of galaxy formation, z_f , which, in principle, can also be constrained.

In theory, a survey large and deep enough to resolve this degeneracy between constant and evolving bias might also enable a model-dependent determination of b_1 and b_2 solely from measurements of S_3 , as described in §2.1. Since distinctions between evolving and non-evolving bias, such as those drawn in Figure 12, could also be made by considering the redshift dependence of S_3 , we can infer that such a survey might address the various degeneracies between b_1 , b_2 , and their evolution, solely from measurements of the skewness, without the need to consider the configuration dependence of the full 3PCF. Unfortunately, it is unlikely that upcoming redshift surveys will be both deep and large enough to resolve the degeneracy of ζ with respect to constant vs. evolving bias, and in any case would still be susceptible to redshift distortions which mix the density and velocity fields. However, BKJ show that the angular 3PCF, which can be well-sampled over a large range of redshifts (e.g., by radio surveys) and is free of such distortions, might be better able to discriminate between evolving and non-evolving bias scenarios.

Based on these results, it is clear that the often-stated result that Q is a constant of order unity (Groth & Peebles 1977; Jing & Zhang 1989; Tóth, Hollósi, & Szalay 1989; Gott, Gao, & Park 1991; Jing, Mo, & Börner 1991; Baumgart & Fry 1991; Bouchet et al. 1993) is only a crude approximation resulting from a coarse averaging over allowed configurations and systematic errors arising from the normalization convention. Valuable information is lost if the geometric dependence of Q , or more appropriately Q_V , is ignored. We also stress that Figures 9–12, are only illustrations; the statistical leverage gained by considering the full configuration-space variation of the 3PCF as a function of redshift should in principle discriminate between the signatures of gravitational evolution versus bias, independently measure the effective present-day values of b_1 and b_2 , the shape of the power spectrum, and possibly measure the evolution in these quantities and constrain the epoch of galaxy

formation.

4. CONCLUSION

We have derived leading-order results for the normalized spatial skewness and 3PCF, assuming Gaussian ICs, for an arbitrary tracer-mass distribution in flat and open universes, taking into account such features as the scale dependence and linear evolution of the CDM power spectrum and the presence of a possibly evolving (decaying), linear or nonlinear bias, as defined for unsmoothed density fields. The predicted normalized amplitudes, S_3 and Q , for an unbiased tracer mass are in agreement with previous work (Bouchet et al. 1992; Juszkiewicz, Bouchet, & Colombi 1993; FG93; Bernardeau 1994a; Fry 1994; JB97). We extend the FG93 result for S_3 in the case of a nonlinear bias, defined for unsmoothed fields, to include a scale-dependent, leading-order correction which becomes appreciable for positive effective spectral indices, corresponding to scales $R \gtrsim 100 h^{-1}$ Mpc for CDM models. This correction term implies that the value of the nonlinear bias parameter, as defined for smoothed density fields, could generally depend on the adopted smoothing scale. In the unlikely event that S_3 could be measured over scales $R \gtrsim 100 h^{-1}$ Mpc, the presence or absence of this behavior could shed light on the smoothed vs. unsmoothed biasing picture, and perhaps allow more accurate determinations of the linear- and nonlinear-bias parameters on the basis of skewness measurements alone.

We show that the conventional definition of Q gives rise to rapid, non-monotonic variation and divergences which do not arise from the behavior of the 3PCF. We speculate that the large discrepancy between this behavior and that predicted by some N -body simulations is due to a practical bias, arising from the poor normalization convention, in the reconstruction of Q from data, rather than from the absence of nonlinear corrections in the QL PT prediction. We propose that this question may be addressed by considering N -body results at earlier cosmic epochs. We consider instead Q_V , which is everywhere well-behaved.

We find the bias model to be a crucial factor influencing the clustering predictions, in agreement with Matarrese et al. (1997). In particular, the scale dependence of S_3 and the configuration dependence of Q_V bear characteristic imprints of bias, such as a relative flattening and decrease with increasing b_1 and a relative increase with increasing b_2 . Unlike S_3 , the predictions for Q_V are seen to depend significantly on the adopted CDM model, through the dependence on Γ , and for all models investigated, the dependence of the 3PCF on triangle geometry implies stronger clustering of smaller, elongated structures. The statistic S_3 , while preserving information about the overall scale dependence, is seen to provide only one test on the combination of the cosmological parameters, $b_1(t)$, and $b_2(t)$,

yielding degeneracies between these quantities, particularly for smoothing scales $R < 100 h^{-1}$ Mpc. These are partially alleviated by considering the dependence of the full 3PCF on the triangle geometry. In particular, the variation of Q_V can be used to distinguish between the effects of gravitational evolution and bias, place constraints on the value of Γ , and measure the effective constant bias terms b_1 and b_2 . Evolving-bias models, however, are found to yield similar predictions for both Q_V and S_3 as models with an appropriately smaller, constant bias, and thus cannot be reliably distinguished using spatial statistics at $z = 0$. Measurements of the 3PCF as a function of redshift could, in principle, directly measure bias evolution, Ω_0 , and the redshift of galaxy formation, but these might be more readily measurable using angular statistics (BKJ). A comparison of these predictions for S_3 and Q_V with several data sets characterizing different tracer populations would allow multiple, complementary constraints on the above parameters. The often-quoted “empirical” result, that the normalized 3PCF is a constant of order unity, is in part a result of coarse-averaging over all triangular configurations, which destroys much of this valuable information.

In practice, other factors arise when comparing these predictions with observations. For example, redshift distortions, which mix information about the density and velocity distributions, must be accounted for when measuring spatial clustering (Fry & Gaztañaga 1994; Jing & Börner 1998; Verde et al. 1998; Heavens, Matarrese, & Verde 1998; Scoccimarro, Couchman, & Frieman 1998). Finite-volume and boundary effects, as well as estimation biases, tend to reduce the observed clustering amplitude (Baugh, Gaztañaga, & Efstathiou 1995; Szapudi & Colombi 1996; Colombi, Szapudi, & Szalay 1998; Gaztañaga & Bernardeau 1998; Hui & Gaztañaga 1998), and Poisson noise (Gaztañaga 1994) and sampling variance must also be taken into account. In addition, the calculations above can be extended in various ways. Our assumed model for the bias is deterministic, but other stochastic models have been proposed which may yield different results, particularly on smaller scales (FG93; Catelan et al. 1998; Catelan, Matarrese, & Porciani 1998; Taruya, Koyama & Soda 1998). One might also investigate the effects of including higher-order nonlinear terms in the PT expansion, such as one-loop results (Jain & Bertschinger 1994; Scoccimarro & Frieman 1996a,b; Scoccimarro et al. 1998); these are expected to be negligible on QL scales, but become increasingly important when comparing predictions with observations on scales where $\xi \gtrsim 1$. For example, N -body simulations indicate that Q becomes relatively shape-independent in the nonlinear regime, suggesting that a linear bias is not the only mechanism capable of producing a flattening (Scoccimarro et al. 1998), and Gaztañaga & Bernardeau (1998) also find that nonlinear effects tend to increase S_3 while erasing the shape dependence of Q . Calculations analogous to those presented here can also be performed for higher-order moments and n -point CFs (e.g., kurtosis, four-point

correlation function, etc.) which, in principle, should provide additional constraints. Finally, the entire discussion can be extended to include the predictions of structure-formation models with non-Gaussian ICs, such as topological-defect or isocurvature models (e.g., Jaffe 1994).

We are grateful to Roman Scoccimarro for numerous discussions and useful suggestions. We also wish to thank Licia Verde, as well as the anonymous referee, for providing helpful comments. This work was supported by a D.O.E. Outstanding Junior Investigator Award, DEFG02-92-ER 40699, NASA NAG5-3091, NSF AST94-19906, and the Alfred P. Sloan Foundation.

REFERENCES

- Baugh, C. M., Gaztañaga, E., & Efstathiou, G. 1995, MNRAS, 274, 1049
- Baumgart, D. J. & Fry, J. N. 1991, ApJ, 375, 25
- Bardeen, J. M., et al. 1986, ApJ, 304, 15
- Bartlett, J. G. et al. 1998, Fundamental Parameters in Cosmology, Les Arcs; Publisher: Editions Frontieres, p. 103
- Bernardeau, F. 1994a, ApJ, 433, 1
- Bernardeau, F. 1994b, A&A, 291, 697
- Bernardeau, F. 1995, A&A, 301, 309
- Bouchet, F. R., et al. 1992, ApJ, 394, L5
- Bouchet, F. R., et al. 1993, ApJ, 417, 36
- Bouchet, F. R., et al. 1995, A&A, 296, 575
- Bouchet, F. R. & Hernquist, L. 1992, ApJ, 400, 25
- Bouchet, F. R., Schaeffer, R., & Davis, M. 1991, ApJ, 383, 19
- Buchalter, A., Kamionkowski, M., & Jaffe, A. 1999 (BKJ), ApJ, submitted
- Cappi, A. & Maurogordato, S. 1995, ApJ, 438, 507
- Catelan, P., et al. 1995, MNRAS, 276, 39
- Catelan, P., et al. 1998, MNRAS, 297, 692
- Catelan, P., Matarrese, P., & Porciani, C. 1998, ApJ, 502, L1
- Colombi, S., Bouchet, F. R., & Hernquist, L. 1996, ApJ, 465, 14

- Colombi, S., Szapudi, I., & Szalay, A. 1998, MNRAS, 296, 253
- Cress, C. M. & Kamionkowski, M. 1998, MNRAS, 297, 486
- Frieman, J. A. & Gaztañaga, E. 1994, ApJ, 425, 392
- Fry, J. N. 1984, ApJ, 279, 499
- Fry, J. N. 1994, PRL, 73, 215
- Fry, J. N. 1996, ApJ, 461, L65
- Fry, J. N. & Gaztañaga, E. 1993, ApJ, 413, 447
- Fry, J. N. & Gaztañaga, E. 1994, ApJ, 425, 1
- Fry, J. N., Melott, A. L., & Shandarin, S. F. 1993, ApJ, 412, 504
- Fry, J. N., Melott, A. L., & Shandarin, S. F. 1995, MNRAS, 274, 745
- Fry, J. N. & Scherrer, R. J. 1994, ApJ, 429, 36
- Gaztañaga, E. 1992, ApJL, 398, L17
- Gaztañaga, E. 1994, MNRAS, 268, 913
- Gaztañaga, E. & Baugh, C. M. 1998, MNRAS, 294, 229
- Gaztañaga, E. & Bernardeau, F. 1998, A&A, 331, 829
- Gaztañaga, E., Croft, R. A. C., & Dalton, G. B. 1995, MNRAS, 276, 336
- Gaztañaga, E. & Frieman, J. A. 1994, ApJ, 437, L13
- Goroff, M. H., et al. 1986, ApJ, 311, 6
- Gott, J. R., Gao, B., & Park, C 1991, ApJ, 383, 90
- Gradshteyn, I. S. & Ryzhik, I. M. 1980, Table of Integrals, Series, and Products (Academic Press, New York)
- Groth, E. J. & Peebles, P. J. E. 1977, ApJ, 217, 385
- Heavens, A. F., Matarrese, S., & Verde, L. 1998, astro-ph/9808016, MNRAS, in press
- Hui, L. & Gaztañaga, E. 1998, astro-ph/9810194, ApJ, submitted
- Jaffe, A. H. 1994, Phys. Rev. D, 49, 3893
- Jain, B. & Bertschinger, E. 1994, ApJ, 431, 495
- Jenkins, A. et al. 1997, Dark and Visible Matter in Galaxies, ASP Conference Series, Vol. 117
- Jing, Y. 1997, Proceedings of IAU Symposium 183, Cosmological parameters and the evolution of the Universe, August 18-22, Kyoto

- Jing, Y. & Börner, G. 1997 (JB97), A&A, 318, 667
- Jing, Y. & Börner, G. 1998, ApJ, 503, 37
- Jing, Y., Mo, H. J., & Börner, G. 1991, A&A, 252, 449
- Jing, Y. & Zhang, J. 1989, ApJ, 342, 639
- Juszkiewicz, R., Bouchet, F. R., & Colombi S. 1993, ApJ, 412, L9
- Kamionkowski, M. & Buchalter, A. 1998, astro-ph/9807211, ApJ, in press
- Martel, H. 1995, ApJ, 445, 537
- Matarrese, S., Verde, L., & Heavens, A. F. 1997, MNRAS, 290, 651
- Matarrese, S. et al. 1997, MNRAS, 286, 115
- Matsubara, T. & Suto, Y. 1994, ApJ, 420, 497
- Mo, H. J. & White, S. D. M. 1996, MNRAS, 282, 347
- Peacock, J. A. 1997, MNRAS, 284, 885
- Peebles, P. J. E. 1974, ApJ, 189, L51
- Peebles, P. J. E. 1975, ApJ, 196, 647
- Peebles, P. J. E. 1980, The Large-Scale Structure of the Universe, (Princeton Univ. Press, Princeton)
- Peebles, P. J. E. & Groth, E. J. 1975, ApJ, 196, 1
- Scoccimarro, R., Couchman, H.M.P., & Frieman, J. A. 1998, astro-ph/9808305, ApJ, accepted
- Scoccimarro, R. & Frieman, J. 1996a, ApJ Supp., 105, 37
- Scoccimarro, R. & Frieman, J. 1996b, ApJ, 473, 620
- Scoccimarro, R., et al. 1998, ApJ, 496, 586
- Steidel, C. et al. 1998, ApJ, 492, 428
- Szalay, A. S. 1988, ApJ, 333, 21
- Szapudi, I. & Colombi, S. 1996, ApJ, 470, 131
- Taruya, A., Koyama, K., & Soda, J. 1998, astro-ph/9807005, ApJ, accepted
- Tegmark, M. & Peebles, P. J. E. 1998, ApJ, 500, L79
- Tóth, G., Hollósi, J., & Szalay, A. S. 1989, ApJ, 344, 75
- Verde, L., et al. 1998, astro-ph/9806026, MNRAS, in press

Watson, G. N. 1966, Theory of Bessel Functions (Cambridge Univ. Press, Cambridge)